Title
Direct 3D Printing of Silicone for Maxillofacial Prostheses

Author
Lee, Yun Chang

Publication Date
2019

Peer reviewed|Thesis/dissertation

UNIVERSITY OF CALIFORNIA

Los Angeles

Direct 3D Printing of Silicone for Maxillofacial Prostheses

A dissertation submitted in partial satisfaction of the

requirements for the degree Doctor of Philosophy

in Mechanical Engineering

by

Yun Chang Lee

2019

ABSTRACT OF THE DISSERTATION

Direct 3D Printing of Silicone for Maxillofacial Prostheses

by

Yun Chang Lee

Doctor of Philosophy in Mechanical Engineering

University of California, Los Angeles, 2019

Professor Pei-Yu Chiou, Co-Chair

Professor Benjamin M. Wu, Co-Chair

Maxillofacial prostheses are state of art and science to help the patient to overcome acquired head and neck defects and bring them back to their daily routine and social life [1]. Silicone prostheses were introduced at 1960 by Barnhart and exhibited excellent combination of mechanical property, chemical resistance, and stability. However, fabrication of maxillofacial prostheses required multiple labor intense process with human interventions, which hindered accessibility of maxillofacial prostheses to patient. The recent digital processing reduced processing time and required number of patient visits significantly on case studies, but direct 3D printing of silicone prostheses was limited due to non-suitable current 3D printing materials with disadvantages such as poor resolution, single color availability, and instability. Therefore, objective of this research was development of direct silicone 3D printing technology for

maxillofacial prostheses with full color 3D printing, proper mechanical properties, complex details availability, and weathering resistance.

In the first study, silica treated silicone powder coated with polymer with hydroxyl functional group and compatible binder system was tested. The polymer coated powder was printed with binder to create porous structure and infiltrated with silicone resin to transform the structure to fully dense parts. This work suggests binder jetting approach on polymer coated silica treated silicone powder, compatible binder system, and silicone infiltration allows direct 3D printing of highly flexible silicone.

Morphology and size of polymer encapsulated silica treated silicone powder was successfully controlled by Ohnesorge number based approach, and the printed parts shows high flexibility with adequate mechanical properties. In clinical testing, the printed ear prosthesis proved complex detail and contour matching requirement. Thus, this study suggests binder jetting of silicone powder strategy is promising for maxillofacial prostheses application.

Cyan, magenta and yellow pigment binders were engineered and, binder showed full color 3D printing availability in skin color printing and full colored ear prosthesis. Weathering resistance in ultraviolet radiation and moisture condition was proved for color and mechanical property, which guarantee enough life span as maxillofacial prostheses. This work suggests a new polymer coated silicone powder 3D printing approach to improve quality of life for patients with head and neck defects.

The dissertation of Yun Chang Lee is approved

Vijay Gupta

Xiaochun Li

Pei-Yu Chiou, Co-Chair

Benjamin M. Wu, Co-Chair

University of California, Los Angeles

2019

TABLE OF CONTENTS

LIST OF FIGURES

LIST OF TABLES

ACKNOWLEDGEMENTS

First of all, I would like to appreciate to my advisor, Professor Benjamin M Wu, for his guidance, and support in my research. Work in your research group and clinical trial offered me invaluable opportunity to develop skills and eyesight as researcher. I also appreciate for the feedbacks and advices from the committee members, Prof. Eric Chiou, Prof. Vijay Gupta, and Prof. Xiaochun Li in development of this project.

I was received plenty of help from the and encouraged by Wu lab members, which prevented me from losing direction during this project. I appreciate of help from my undergraduates and dental student for preparing and conducting experiment. The clinical trials on UCLA maxillofacial clinic with Dr. Jayanetti, Tomomi, and residents were moment of trues and advices to improve result of 3D printed devices and prostheses.

Last but not least, I want to express gratitude to my family for their sincere support. Without support of them, I could not reach achievement in this thesis project.

VITA

2012	Bachelor of Engineering
	Stony Brook University, New York
2016	Master of Science, Mechanical Engineering
	University of California, Los Angeles
2015-2019	Graduate Student Researcher, Mechanical Engineering
	University of California, Los Angeles
2018-2019	Teaching Assistant
	University of California, Los Angeles

Proceedings

1. C. Cagino, J. Jayanetti, **Y. Lee**, B. Wu, "Case Report: Fabrication of an Interim Nasal Prosthesis via Rapid Prototyping", Poster Presentation at 2016 American Academy of Maxillofacial Prosthetics
2. N. Rojanasakul, T. Baba, **Y. Lee**, J. Jayanetti, "Prosthetic rehabilitation of extensive lower facial defect: case report", Poster Presentation at 2018 American Academy of Maxillofacial Prosthetics

Chapter 1. Introduction to 3D Printing of Silicone Maxillofacial Prostheses

1.1. Background

1.1.1. Abstract

Cancer surgery, trauma, and malformation may lead to broad head and neck defect which are not possible to be covered by patients, and those defects often require rehabilitation by maxillofacial prostheses which help the patient to overcome acquired head and neck defects and brought them back to their daily routine and social life. Silicone based prostheses exhibited high elongation at break, weathering stability, and moderate elastic modulus because of excellent combination of mechanical property, chemical resistance. However, even for currently, most of maxillofacial prostheses are fabricated in conventional process, which involves human intervention for each of steps. As a result, patients are required to visit hospitals more than 5 times and the final delivered time for maxillofacial prostheses is 5-10 weeks after the patients requested maxillofacial prostheses, which hinders accessibility of maxillofacial prostheses to patients. The recent digital based processing reduced processing time and required number of patient visits significantly on case studies, but direct 3D printing of silicone prostheses was limited due to non-suitable current 3D printing materials with disadvantages such as poor resolution, single color availability, and instability.

1.1.2. Development of Maxillofacial Prostheses for Head and Neck Defects

Cancer surgery, trauma, and malformation may lead to broad head and neck defect which are not possible to be covered by patients, and those defects require rehabilitation at all ages [2]. The prosthetic rehabilitation has been suggested as surgical alternatives in functional-aesthetic facial reconstruction if reconstructive surgery approaches are not applicable because of psychophysical conditions of the patient or excessive substance loss [3]. Maxillofacial prostheses

have helped the patient to overcome acquired head and neck defects and brought them back to their daily routine and social life [1]. The use of maxillofacial prostheses at early stage with natural wax and precious metals was reported for Egyptian mummies, and early Chinese with natural waxes and resin, gold, and silver [4].

The researches to develop optimal material system for maxillofacial prostheses had been conducted, and first silicone based prosthesis was introduced at 1960 by Barnhart [5]. Silicone based prostheses exhibited high elongation at break, weathering stability, and moderate elastic modulus [1]. Excellent combination of mechanical property, chemical resistance, and stability made silicone became popular for extraoral prostheses applications [1]. As followed by development of technic and understanding about maxillofacial material, the problem reported by wearer or patients were reduced, and fully customized prosthesis for each patient was allowed [2].

Even for currently, most of maxillofacial prostheses are fabricated in conventional process, which involves human intervention for each of steps [6]. The summarized process for fabrication of maxillofacial prosthesis for conventional and digital based approach is suggested on Fig.1-1. Because maxillofacial prostheses require multiple step for impression mold making and need curing time for casting mold and silicone, patients are required to visit hospitals more than 5 times and the final delivered time for maxillofacial prostheses is 5-10 weeks after the patients requested maxillofacial prostheses [7]. The total estimated cost for maxillofacial prostheses is $15,000 [8] and can be increase even more depending on various condition, such as size of trauma.

To overcome drawback of conventional maxillofacial prostheses fabrication process, use of digital processing based on 3D scanning and 3D printing has been suggested and utilized. The digital based processing reduced processing time and required visit of patient significantly on case study [6]. The total cost of processing was reduced to one third of original cost while satisfying

patients demands [9]. Digital based processing for maxillofacial prostheses is divided to direct 3D printing without fabrication of molds and indirect 3D printing to create mold to cast silicone. For indirect mold fabrication, facial replica production approach for digital processing is depicted on Fig. 1-2 and Fig. 1-3. 3D printing of silicone mold approach is described on Fig. 1-4. Indirect 3D printing to create molds reduced delivery time compared to the conventional methods recently, and direct 3D printing of silicone maxillofacial prostheses will bring cost and time even more [10]. However, obstacles such as the lack of established 3D printing techniques for handling of viscous medical grade silicone resin and incompatibility of the 3D printing system hindered development and utilization of direct 3D printing of silicone for prostheses [10]. Thus, the researches and developments about direct 3D printing of silicone for maxillofacial prostheses are highly required.

1.1.3. Stereolithography (SLA) based 3D printing of Silcone

Stereolithography or Stereolithography Apparatus is the 3D printing technic to create parts on vat of Ultraviolet light curable resin by projection or scanning of cross section of desired parts with UV light sources as shown on Fig.1-5. Improved SLA system was recently suggested using focused UV light beam and formation of structure on the middle of the vat to prevent breakage and deformation of structure during reflow of high viscosity resin on the building area [11]. Minimal movement and swirling on the resin vat are induced in this technic, which creates a hydrostatic environment which acts as a support structure shown on Fig.1-6. This support-free fabrication technique requires a complex UV light source and precise control the light intensity. However, the viscosity limit and control require additional study for development and utilization with medical grade silicone, which limit its application to low molecular weight silicone with low viscosity and low mechanical strength. Moreover, removing captured air or gas in hydrostatic silicone vat to create defect-free printed parts is challenging and, the reported resolution of this

technic is 1–2 mm which is still too low for maxillofacial prostheses. Therefore, low resolution, distortion, and defect in the printed layer hinder fabrication of complex shape structure required for maxillofacial prostheses.

Commercialized silicone-urethane copolymer by Carbon3D® introduced in 2017, which could create high resolution parts with 30A hardness, even though it require support structure for printing overhang, thin edge, and complex shape [12]. Among SLA technic, Digital Light Processing system was used for 3D printing of polyurethane-silicone copolymer which is based on micro-mirror array to control area of UV projection in tenth of micron size of pixel and allowed precise control of UV exposure. However, silicone-urethane copolymer exhibit unstable material characteristic due to urethane functional group on polymer, and showed degradation and unstable property by weathering in vivo condition [13]. Degradation of polyurethane polymer and copolymer is affected by hydrogen peroxide and enzyme formed by microbials [14]. This low degradation resistant property limits the use of SLA 3D printed silicone prostheses because maxillofacial prostheses are frequently exposed to moisture and UV light which form hydrogen peroxide by wearing of maxillofacial prostheses in outdoor. Also, the degradation and contamination by microbial would be undesirable, which lead to unwanted inflammation or microbial attack on patients. The unstable color characteristic and low bonding strength for adhesive retained prostheses was also reported for polyurethane contained prostheses [1].

In addition, mishandling in polyurethane prostheses in moist condition lead to presence of diisocynates in prostheses which shows toxicity and defect such as pores [1]. Thus, color and mechanical stability in topical use of patient is not satisfied for current silicone-polyurethane copolymer. Last but important, only single material in vat is used for SLA technic, which cannot

satisfy full- color 3D printing which is highly required for direct 3D printing of silicone for maxillofacial prostheses to match color of prostheses with patient skin shade.

Thus, the SLA printed prostheses are required manual color mixing on the printing material and touch up with silicone colorant, which limit application of direct 3D printed prostheses and additional time and cost for manual processing. Thus, SLA approach for 3D printing of silicone is only limited to single color printed prostheses with limitation in dimensional accuracy or stability.

1.1.4. Embedded 3D printing of Silicone base Approach for Silicone

Embedded 3D printing of silicone is extrusion and vat-based process which described as directly writing inks into matrix materials [15]. In this process, silicone resin and crosslinker is extruded out from syringe needle to shear-thinning fluid which creates hydrostatic environment and acts as support material for printing. As a result, lines of crosslinked silicone resin are suspended on shear thinning fluid as shown on Fig. 1-7. By scanning the area with syringe need to controlled speed of extrusion to form a layer and repeating this process for each of the layer, 3D volumetric parts are created. It is also possible to print with multi-material by using set or array of syringe nozzles. Also, by using silicone resin as support structure and cure all materials together to create multi-material parts with intended functionality such as sensor or color. However, one of the drawbacks in this technology is severe trade off characteristic between printing speed and resolution, which limit its application to lab-scale research. Reported resolution for this 3D printing technic is 140-400um with 20mm/s of line printing speed [16].

To minimize defect and optimize quality of printed parts, approach based on expert-guided optimization process for embedded 3D printing was suggested [17]. However, it still showed severe warping and distortion in parts as shown on Fig.1-8. The main factor related to distortion

and defect of embedded 3D printing is related to shear thinning behavior of fluid in reservoir and induced air pocket during printing as shown on Fig.1-9. As the viscosity increase for shear thinning fluid, the fluid supports the printed layer and parts with minimized displacement of printed region but, increase in viscosity results in larger air pocket behind the needle which induces air bubble and distortion in printed parts. Also, movement of syringe needle in fluid reservoir result in swirling of printed structure also. Last but important, because this technic have limitation in precise deposition of base color with high enough resolution, full-color 3D printing requirement is not satisfied with this approach which require to match color of prostheses with patient skin shade. Thus, the embedded 3D printing is still limited to lab scale for test single and multi-material with limitation in geometry and shape, which limit application to clinical use of direct 3D printed prostheses

1.1.5. Direct Jetting of Silicone by Drop on Demand Approach

Wacker Chemie AG introduced silicone printing system with drop on demand control in 2015 [18]. In this approach, droplets of UV curable silicone and support material are deposited to build platform and cured by UV light radiation immediately as described on Fig.1-10. The printed parts are postprocessed to remove support material and cure silicone material completely in elevated temperature condition. This approach has advantage in multi-material availability by using array of droplet printheads but have limitation in resolution. The reported maximum resolution for this technology is 400um in z-axis direction and inaccurate marginal matching with contour of facial defects [19].

Also, printing layer step lines were not possible to completely hidden after polishing and coating as suggested on Fig. 1-11. The main difficulty of this technology is associate with high viscosity characteristic of medical grade silicone, which hinder the stable droplet generation and

nozzle size for printing [10]. In addition, high resolution with precise deposition control is required for full color 3D printing, as study about photocuring acrylic material suggested [20]. Thus, the approach based on direct deposition of silicone is not currently possible to print with high enough resolution and full color control require as maxillofacial prostheses.

1.1.6. Binder Jetting approach for 3D printing of Silicone

Binder Jetting is the powder-based 3D printing approach to create volumetric parts. In binder jetting, powder is fed to the platform and evenly spread by the roller [21]. Then printheads deposit droplets on the top surface powder bed and make connection between particle as shown on Fig.1-12. These connections create a cross sectional layer of 3D model, and this process is repeated until complete volumetric parts is prepared. The initial printed parts directly come out from powder possess pores in structures and are recommend filling the pores with other material by infiltration process to improve mechanical property. In infiltration process, other material in liquid phase such as polymer or metal wet the porous structure of printed parts and turn the initial green parts to fully dense parts.

The recent studies in binder jetting approach for maxillofacial prostheses utilize starch for initial green parts and infiltrated with medical grade silicone to create starch-silicone composite [22]. The starch based binder jetting approach offered full color 3D printing availability with complex details [23, 24] and reasonable cost ranges [25]. Also, biocompatibility was proved in Alamar blue cell assay. However, the 3D printed parts on starch material system show limited integration between silicone and starch. Also, natural weathering in 6 weeks of outdoor exposure leads to severe degradation in color, and mechanical property degraded by moisture easily [22]. Therefore, the application and life span of this starch-silicone composite material is quite limited to temporary prostheses.

1.1.7. Conclusion

Among current silicone 3D printing technology, only binder jetting technology can offer reliable formation of complex structure required as maxillofacial prostheses without support structure. Also, binder jetting approach is the only approach proved full color 3D printing availability of silicone material. However, the current material system for binder jetting of silicone is vulnerable to UV and moisture induced weathering, which limit the application as the maxillofacial prostheses.

1.2. Research Objectives

Thus, binder jetting approach with new material system to create fully flexible silicone prostheses is promising. The objective of this research is to design binder jetting based 3D printing material system that allows direct 3D printing of silicone for maxillofacial prostheses with full color 3D printing availability, high flexibility, and stable color and mechanical property. This objective was accomplished by completing the following specific aims which were elaborated in Chapter 2, 3, and 4.

Aim 1: To develop Biocompatible 3D Printing Material System which can print with complex shape of maxillofacial Prostheses

A. To develop with biocompatible binder, silicone powder, and medical grade silicone for 3D printing and postprocessing.

B. To test with clinical case to check possibility of complex shape printing and match with contour of patient defect region.

Aim 2: To develop highly flexible structure with proper mechanical properties

A. To develop infiltration process to change porous silicone powder structure to fully dense part

B. To investigate mechanical property of infiltrated parts with high elongation at break (>400%) and moderate elastic modulus.

Aim 3: To develop Full Color 3D printing binder for customizable skin shade printing.

A. To develop and test Cyan-Yellow-Magenta pigment dispersion system for organic solvent binder.

B. To investigate and fabricate full color skin shaded sample and proof of concept prostheses.

Aim 4: To develop Weathering and Fatigue Resistance Silicone 3D printed Material

A. To develop and test with UV resistance silicone and pigment material system for color 3D printing.

B. To investigate and characterize effect on fatigue loading on 3D printed material.

1.3. Innovations

- This thesis project suggested first silica treated silicone powder-based binder jetting approach and proved possibility of printing of complex contour with its material system.
- Development of the new material system involved first clinical trial of silicone powder printed prostheses on patient and showed compatibility with current silicone colorant, coating, and adhesive system for clinical use.
- No study suggested organic solvent binder with Poly Vinyl Butyral coated powder for binder jetting system. This unique combination of material allowed its weathering resistance about moisture in color and mechanical property
- Full color 3D printing availability about silicone powder 3D printing system for custom skin shade and proof of concept prostheses with full color was firstly introduced
- Weathering resistance about silicone composite fabricated by binder jetting approach was proved for enough life span as maxillofacial prostheses

- This study first approach about control of spray dried polymer coated silicone powder property based on Ohnesorge number, which allowed customized polymer silicone powder for biomaterial fabrications.

1.4. Figures

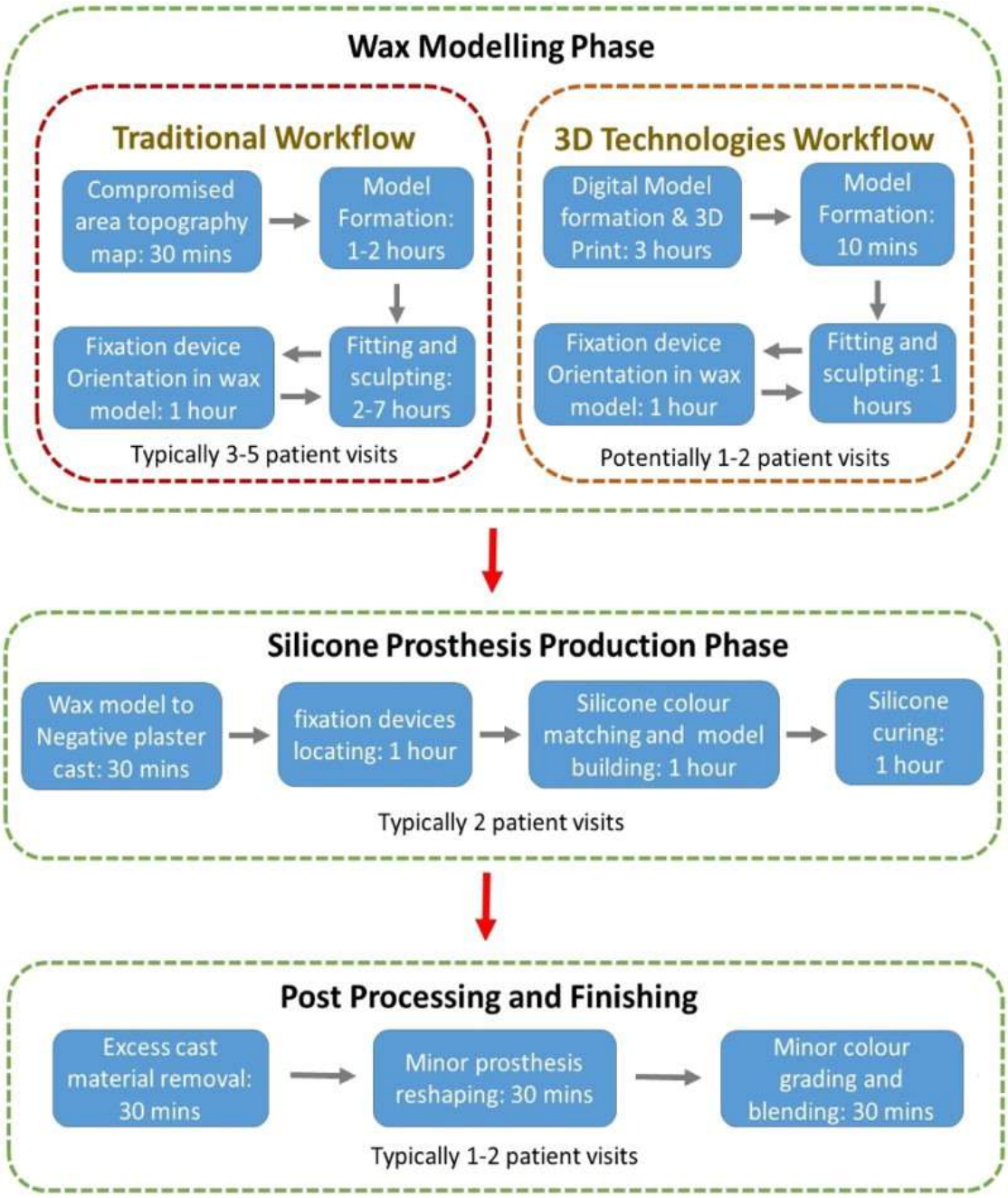

Figure 1-1. Comparison Between Conventional and Digital Based Processing for Maxillofacial Prostheses. Reproduced with permission from [9].

Figure 1-2. (a-d) Digital Based Ear Replica and Mold Fabrication processing for Maxillofacial Prostheses. Reproduced with permission from [9].

Figure 1-3. (a-c) Painting and Color Matching process for Maxillofacial Prostheses. Reproduced with permission from [9].

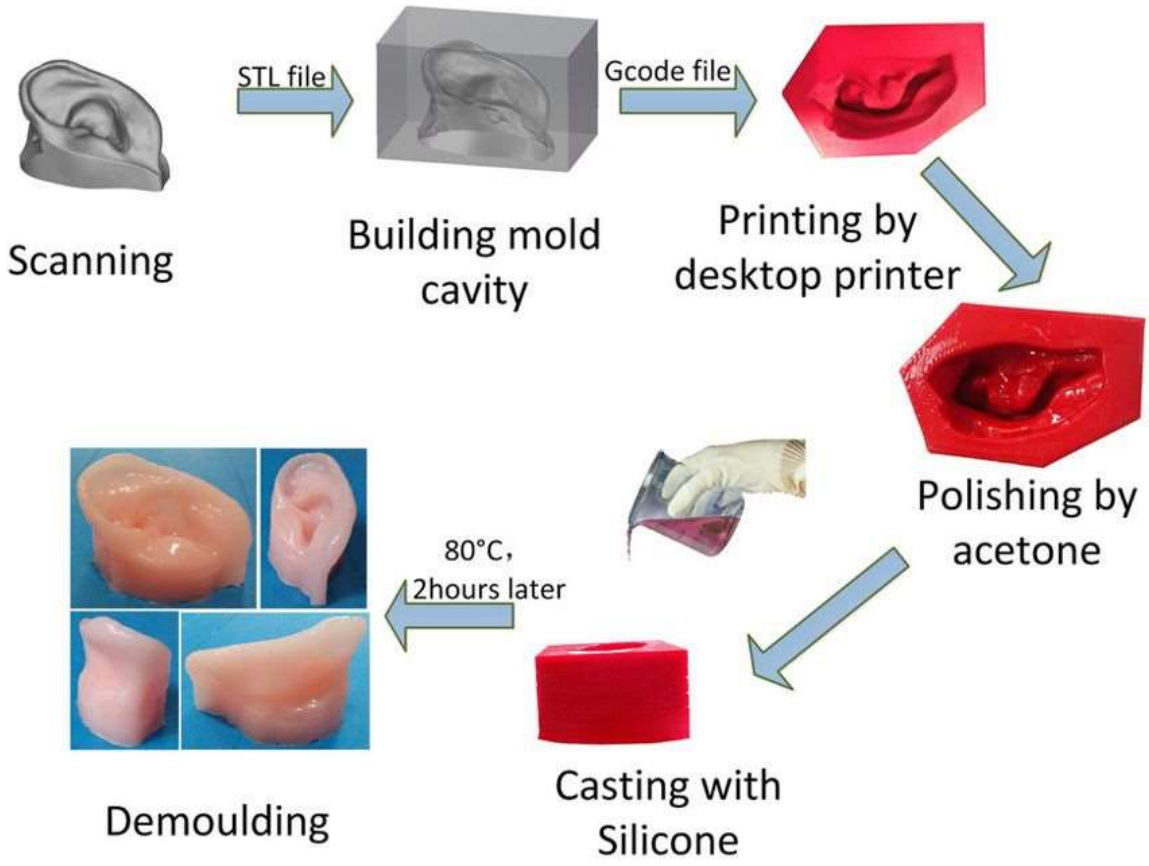

Figure 1-4 3D Printed Mold Fabrication Process based on Fused Deposition Modeling. Reproduced with permission from [7].

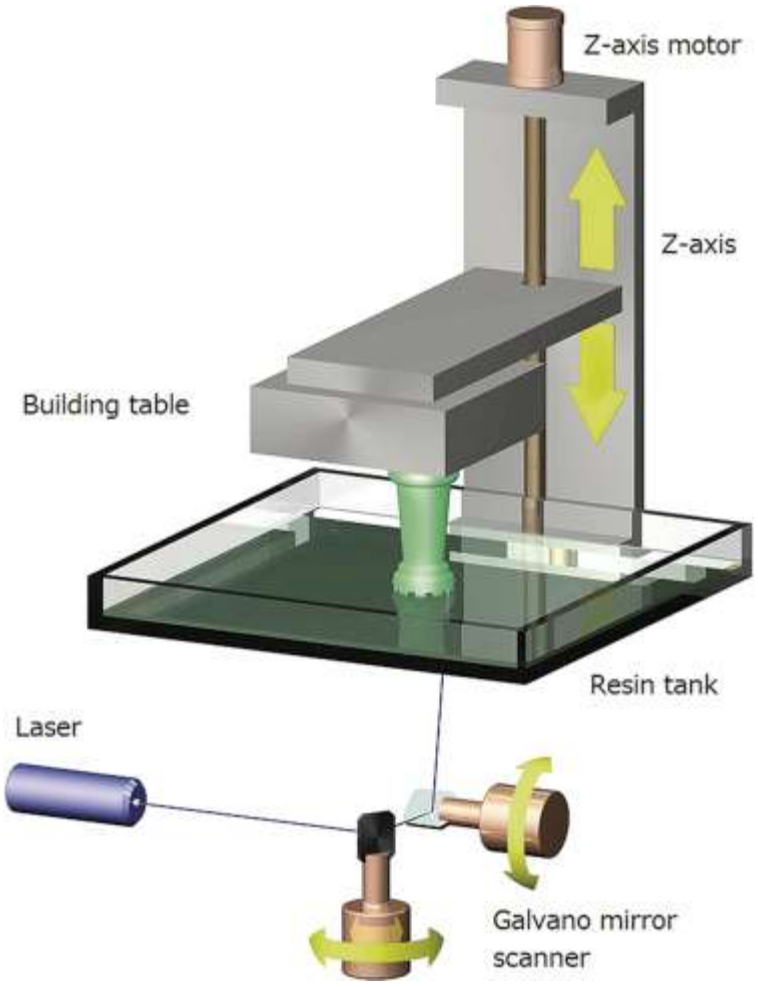

Figure 1-5. Scheme and Printed parts for SLA technic. Reproduced with permission from [26].

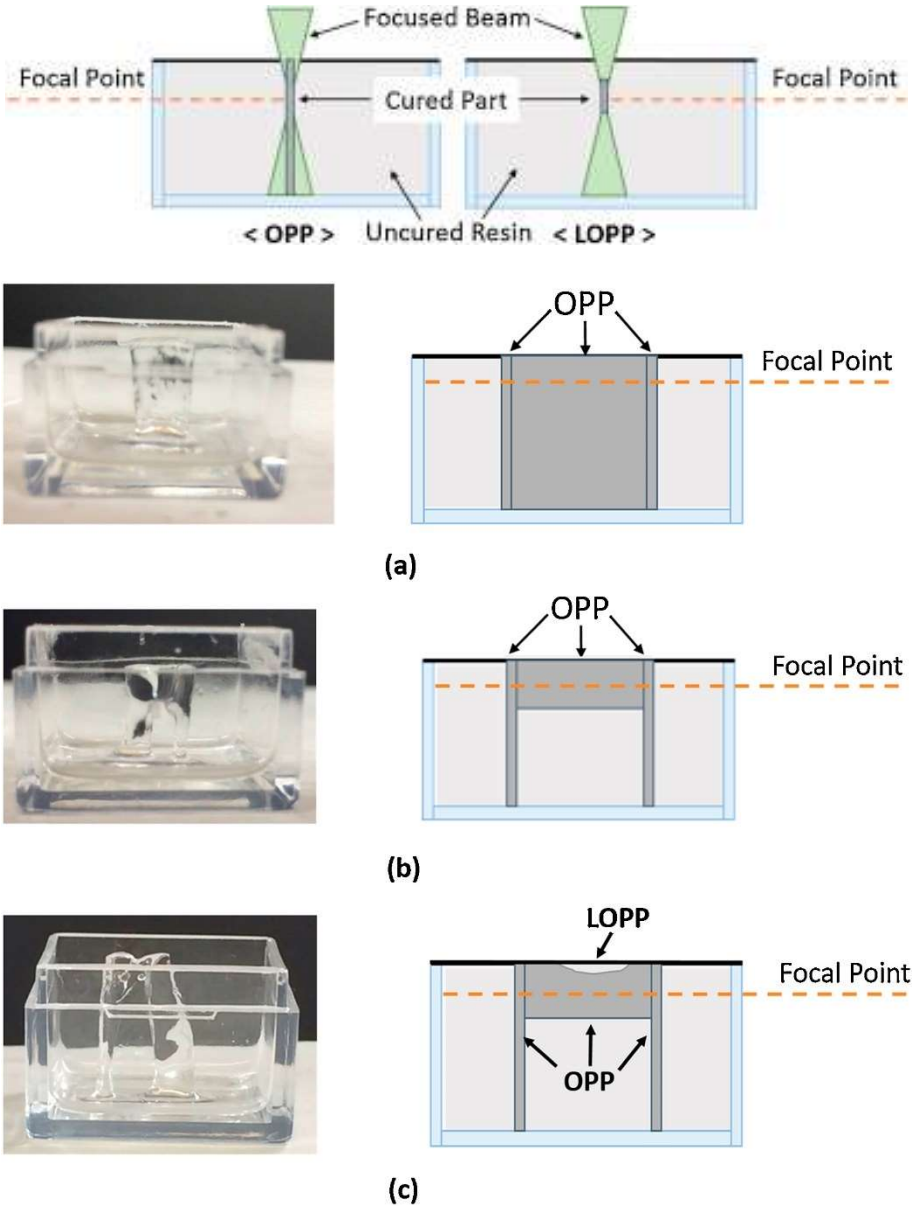

Figure 1-6. Scheme and Printed parts for Advanced SLA technic, (a-c) one-photon polymerization (OPP) and low one-photon polymerization (LOPP). Reproduced with permission from [11].

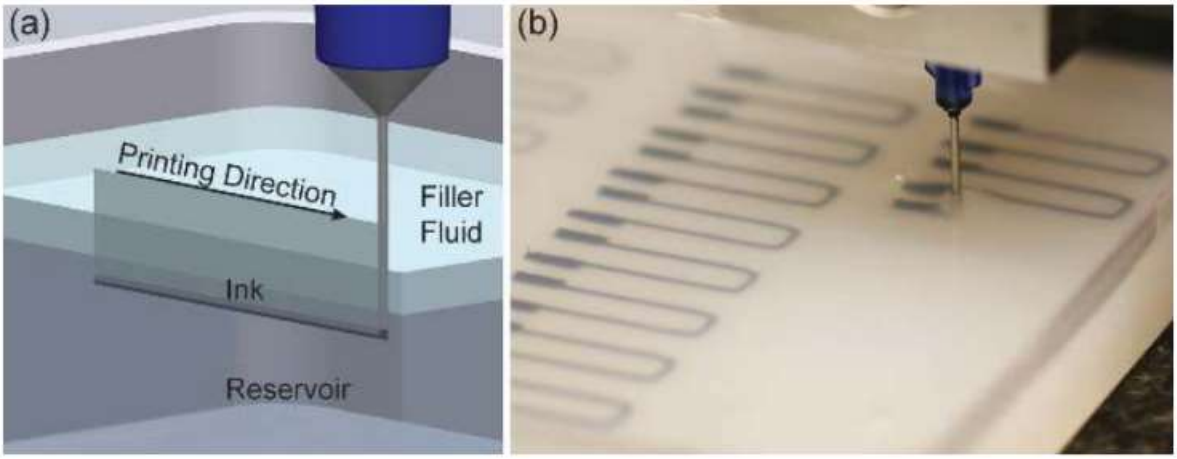

Figure 1-7. (a)Scheme and Printed parts for Embedded 3D printing. (b)fabrication of multi-material parts for stain sensor application. Reproduced with Permission from [27].

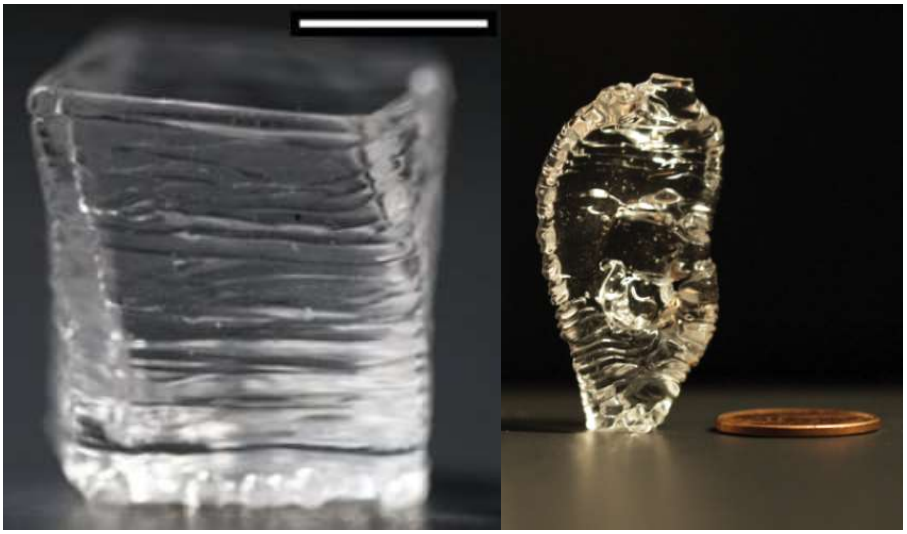

Figure 1-8. Distortion and Defect on Embedded 3D printed Parts. Reproduced with Permission from [17].

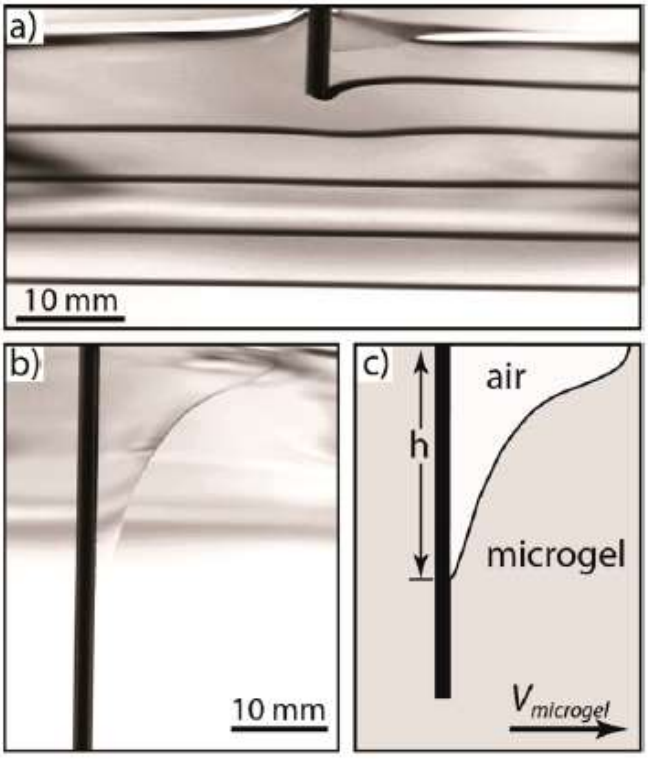

Figure 1-9. Distortion and Defect phenomenon by Induced Air pocket in Embedded 3D printed Parts. Reproduced with Permission from [28].

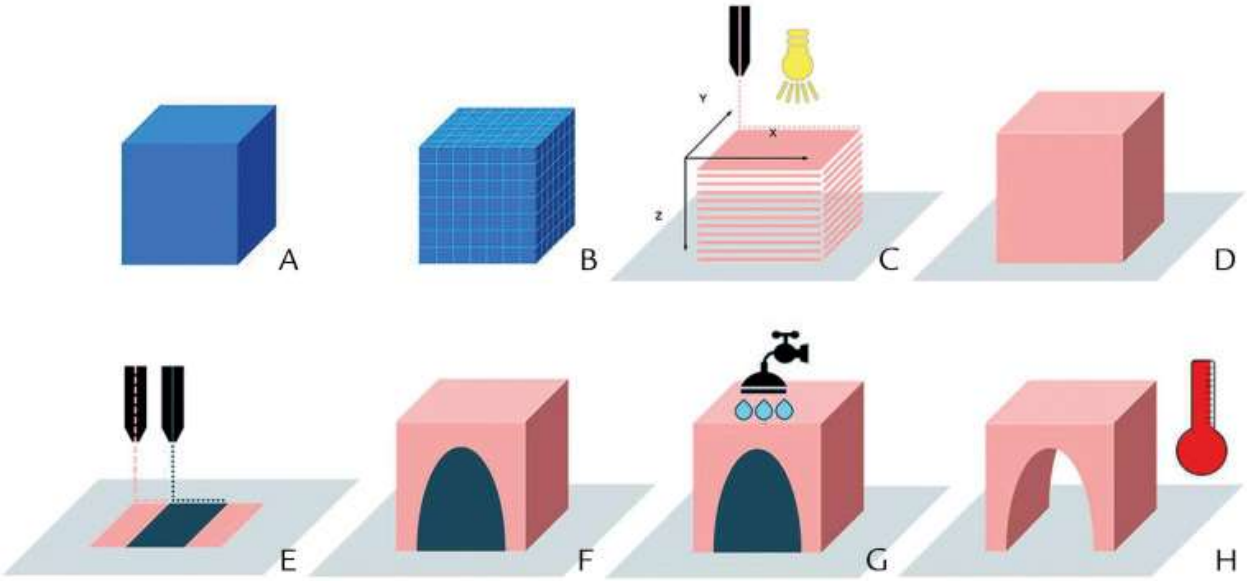

Figure 1-10. (A-H) 3D printing Process for Direct Jetting of Silicone Parts. Reproduced with Permission from [19].

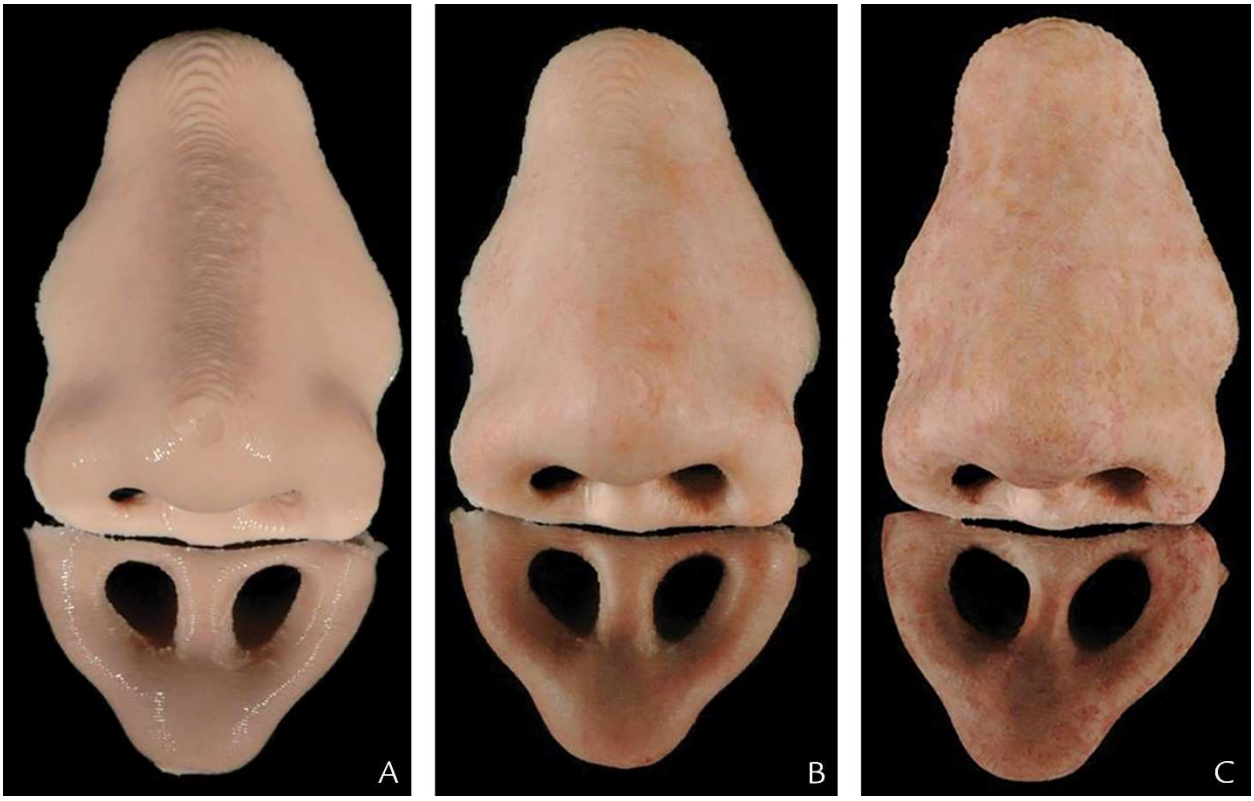

Figure 1-11. (A) Initial Printed Prostheses from Direct Jetting of Silicone approach. (B)Painted Part with colorant. (C). Finished parts with Coating and Polishing. Reproduced with Permission from [19].

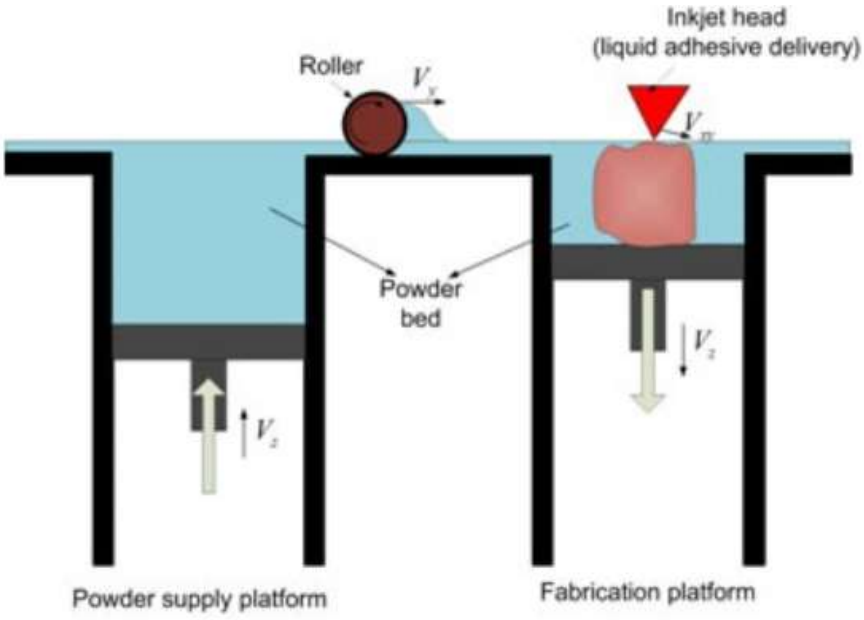

Figure 1-12 Schematic Diagram of Binder Jetting Approach. Reproduced with Permission from [21].

Figure 1-13. Nasal Prostheses fabricated based on Binder Jetting Approach. Reproduced with Permission from [24].

Chapter 2. Development of Initial Silicone Powder Material System

2.1. Abstract

In this chapter, silica treated silicone powder based material system was tested. Due to inert surface characteristic of silicone powder, it had to possess silica surface layer to interconnect particles with polymer binder and form porous structures as green parts. Polymer with hydroxyl functional group and compatible binder system was tested. The silica treated silicone powder was encapsulated with hydrophilic polymer by spray drying. The polymer coated powder was printed with binder to create porous structure and infiltrated with silicone resin to transform the structure to fully dense parts. Poly Vinyl Butyral 7% coated powder showed high elongation at break over 300%, and this work suggests binder jetting approach on polymer coated silica treated silicone powder, compatible binder system, and silicone infiltration allows direct 3D printing of highly flexible silicone.

2.2. Introduction

Recent study about full color 3D printing of starch-silicone composite maxillofacial prostheses suggest possibility of direct printed silicone maxillofacial prostheses with minimized human intervention, but inhibit unstable color and mechanical characteristic due to embedded starch with poor integration with silicone resin [22]. One of the possible approaches to overcome limitation of material would be replacing material to the other one with high weathering resistance and proper integrity with silicone infiltrant. Silicone powder satisfied this requirement with biocompatibility on topical use. However, because of its chemical resistance, silicone powder presents inert surface characteristic [29] and hard to form interconnection between particle by dissolving silicone or binder; interconnection between particles are highly required to print porous green structure in binder jetting approach. To overcome inert surface characteristic of silicone,

silica treated silicone powder was selected as main powder material because silica forms hydrogen bonding with polymer with hydroxyl group and interacts with the oxygen atoms of the polymer chains [30]. This unique chemical characteristic of silica helps adhesion of hydrophilic polymers on silica surface to help form porous green structure. To evenly distribute hydrophilic polymers on the powder surface, spray drying process were recommended because the spray drying allow proper encapsulation and particle size control at the same time [31].

2.3. Material and Methods

2.3.1. Development of Polymer Coated Silicone Powder by Spray Drying

The amorphous fumed silica treated bis-vinyl dimethicone/dimethicone copolymer powder (Wrinkle Blur, MakingCosmetics Inc, Snoqualmie, Washington) with 2μm average diameter, 3-7wt% silica ratio, and 1.01g/cm3 density was used for the main powder material. The composition of each powder-polymer mixture is on Table.1. We prepared for 2.4, 4.8, and 7.0wt% polymer ratio Poly Vinyl Butyral and 2.0, 5.0, and 7.0wt% Poly Vinyl Alcohol coated silica treated silicone powder.

The PVB powder solution was prepared by dissolving Butvar®-76 powder (Eastman Chemical Ltd, Kingsport, Tennessee) in Acetone (Fisher Chemical, Pittsburgh, Pennsylvania) via closed flask in an 85 °C water bath for 30 min. After complete dissolution, the mixture was removed from heat and a solution of HPLC grade ethanol (Sigma-Aldrich, St. Louis, Missouri) and DI water were added to the mixture, stirring manually. Silica-treated silicone powder was then distributed into the mixture using a magnetic stir bar and plate for approximately 20 min. The final mixture was stored in a closed poly bottle at room temperature until further use.

The PVA powder solution was prepared by mixing a solid combination of PVA (31,000M.W, Sigma-Aldrich) and silica-treated silicone powder. The dry powder mixture (20 wt%) and Tween-80 (Mallinckrodt Baker Inc. Dublin, Ireland), a non-ionic detergent, were then

dissolved in deionized water at room temperature. The final solution was mixed using a magnetic stir bar for approximately 20 min. Any observed clumping was broken up manually as needed. The mixture was stored in a closed poly bottle at room temperature until use.

The spray drying of the powder mixtures were performed using a Mini Spray Dryer B-191 (BÜCHI Labortechnik AG, Flawil, Switzerland) and a 1.45mm nozzle. The aqueous powder mixture was fed to the droplet atomizer using a length of tubing through a circulating peristaltic pump. Droplets of solution are sprayed through the nozzle into the drying chamber, where the moisture is removed to leave solid particulate. The resultant powders are collected via cyclone and deposited into the collection vessel, where the final powder can be removed for use. Stiff, polyethylene sheets are used to remove excess powders adhered to the interior walls of the drying and cyclone chambers. In instances of excessive powder adhesion to the borosilicate chambers, the collected powders are further filtered using a 500μm sieve to restrict the powder particle size prior to use. The standard preset condition was used for the PVB powder mixture, which maintained the inlet temperature, sample feed rate, and compressed air flow rate at 80 °C, 20%, 800 L/min, respectively at 100% aspiration. The high temperature condition was used for the PVA powder mixture, with the inlet temperature, sample feed rate, and compressed air flow set at 120 °C, 20%, 800 L/min, respectively at 80% aspiration. Composition of spray drying mixture is described at Table.2-1, and schematic diagram of spray drying is described at Fig. 2-1.

2.3.2. Development of Compatible Binder for 3D Printing of Silicone Powder

The base 3D printing binder formulations used for 3D printing consisted of acetone (Fisher Chemical) and HPLC grade ethanol in DeIonized water. FD&C Red #40 powder pigment (ColorCon, Irvine, California) and Pluronic® F-68 (Sigma-Aldrich), a non-ionic surfactant, were added to the binder solutions at concentrations. The solutions were prepared in a conical tube and

vortexed for 1 min, or until homogenous as needed. Excess particulate was filtered from the binder solutions using a 1 μm Polytetrafluoroethylene filter(Fisher Chemical) before loading of the binder into the printhead cartridges for use. For comparison, dilutions of Poly Acrylic Acid (1800M.W, Sigma-Aldrich) and Pluronic® F-68 surfactant in DI water were added in parallel to the above formulation to observe the ballistic effect of the different binder solution viscosities during the 3D printing process.

The viscosity was measured in a rheometer (Discovery HR-2, TA Instruments, New Castle, Delaware) with a 40 mm 2.016◦ plate attachment and shear rate ranging from 25 to 630 Hz in shear sweep method. Average viscosity at 100 Hz data was used to compare the viscosity. The surface tension was observed with a , Kimble Chase 14818 Tensiometer (Cole-Parmer, Illinois). **Equation 1** [32] was used to determine surface tension, γ, where h is the height difference between menisci, r is the inner radius of the capillary, ρ is the density of the solution, and g is acceleration due to gravity. Five measurements were conducted for each measurement of fluid mechanical properties.

$$\gamma = hr\rho g/2 \tag{1}$$

Inverse of Ohnesorge number, Z which reflects the physical properties of the fluid droplet is derived from surface tension γ, viscosity μ, density ρ, and the drop radius d [33].

$$Z = \frac{\sqrt{\rho\gamma d}}{\mu} \tag{2}$$

To create stable droplet, Z >1 is required. If Z>14, the fluid still printable in **Equation 2**, but satellite droplet can form and lower the accuracy of droplet deposition location [33].

A dilution of acetone(5wt%) and Pluronic® F-68 surfactant(0.5wt%) in deionized water was prepared as a cleaning solution for the repurposed HP11 (Hewlett Packard Inc, Palo Alto, California) thermal inkjet printhead cartridges. The septum tube connector and the cap was temporarily removed to wash inside. The cap and printhead cartridge was washed with DI water

thoroughly for 1 minute and with the cleaning solution for 1minute. The cartridge was filled with the cleaning solution using squeeze bottle and apply -0.1bar vacuum on the printhead nozzle. By applying low vacuum, we can remove out remaining pigment and contamination on printhead with minimal damage. The low vacuum cleaning procedure was repeated for 10minutes. Also, a washing solution was prepared to clean the printhead nozzle during self-purging sequence of ZPrinter-510 (3D Systems inc, Rock Hill, South Carolina). Washing solution in purge station was changed to water based solution with Tween-80,(0.25wt%) and ethanol(5wt%) which can wash out possible contamination due to polymeric coating.

A Z510 printer was adapted to print green parts with silica treated silicone powder. Power supply for printhead board was separated to isolated 12V and 5V power source(TDK-Lambda Americas, National City, California), to ensure stable voltage supply during droplet generation. Fluid lines to waste tray were replaced with PTFE tubing to prevent any possible damage or leaking of binder waste. Binder supply lines to printheads were disconnected to use printheads as cartridge to hold binder. To minimize cross contamination of powder, we used separable building platform. It was made of Vero Purewhite®(Stratasys Inc. Eden Prairie, Minnesota), photocurable acrylic resin, with J750 printer(Stratasys Inc.). The build platform was designed to snap-fit and had matched perforated pattern to the original build platform of Z510 printer.

For the printing of binder on silicone powder bed layer, Z510 3D printer was operated in following procedures. First, the build and feed platform of Z510 printer was lowered. Then prepared printheads on the fast axis assembly were installed. The powder was set on the feed piston. Then the powder was packed using flat acrylic plate. The powder was spread by the roller in fast axis and repeating built in spreading function. 0.1mm layer thickness and 21.7% uniform binder

saturation with monochromatic binder option was used for 3D printing. Detailed procedure is described on Fig.2-2.

To measure severity of ballistic effect, 6 set of 10mm circle on the powder layer was printed. The severity of ballistic effect was quantified as ballistic effect diameter difference as on **Equation 3**. The ballistic effect diameter was measure on the seventh layer just after droplets were deposited on to the powder layer shown on Fig.2-2. Five circles with least deformation was chosen for the measurement and tested for each polymer coated powder with the acetone-based binder and PAA binder with different viscosity with silica treated silicone powder combinations. The D_{o} and D_{i} were measured using ImageJ based on **Equation 3**.

$$D_{\mathrm{diff}} = D_{\mathrm{o}} - D_i \tag{3}$$

2.3.3. Characterization of Mechanical Property for Porous and Fully Dense Structure

The disc shaped specimens for mechanical testing are designed to test the elastic modulus of green parts. Due to extreme low elastic modulus of the green parts, it was tested with Dynamic Mechanical Analyzer Q800 (TA Instrument) with strain rate condition. Five samples were tested for each of polymer coated powders. The sample was designed with Solidworks2014 (Dassault Systemes, Vélizy-Villacoublay, France) in 10Φx5t (mm) cylindrical shape and exact dimension of the printed specimen was measured with 6 inch digital caliper (Fowler, Newton, Massachusetts) for stress and strain calculation. The compressional clamp and position of the DMA was calibrated before testing and every two hours due to sensitivity of the samples. Samples were isothermally heated up to 25°C with 1mN preloading condition and compressed in 20% compression/min speed, up to 60% of compression. 40% modulus of the samples were compared.

The tensile sample was designed with Solidworks2014 in 25Lx5wx1t (mm) rectangular bar shape and printed with Z510 printer to form porous green structure. To transform porous green

parts to fully dense parts, infiltration procedure was conducted. The cleaned parts for tensile testing samples were infiltrated with silicone resins, to make them to full dense parts. The two-parts platinum cure silicone, RTV 4420 (Bluestar Silicones USA Corp, East Brunswick, New Jersey), and hexadimethylsiloxane solvent, Novocs Matte (Smooth-On, Inc. Macungie, Pennsylvania) were dispensed to conical tube in 25%, 25%, and 50% ratio by weight. The conical tube was vortexed for 1 minutes or more to evenly mix the contents. Forced wetting condition was applied at 3 bar pressures with compressed air in zinc plate pressurized tank (McMaster-Carr, Elmhurst, Illinois) for 30 minutes. After 30 minutes, the compressed air was released slowly, below 3bar/minutes rate pressure change to prevent possible stress generation. The chamber was connected to vacuum with -0.7 Bar pressure to further increase infiltrated area and remove the solvent. After 30 minutes, we release the vacuum slowly, below 3bar/minutes rate.

The tensile testing was also conducted with the DMA. The exact dimension of the printed and infiltrated samples was measured with digital calipers for stress and strain calculation. The samples were clamped by tensile testing jigs and the clamp in tensile jig was tightened in 0.25N·m with torque driver. The samples were isothermally heated up to 25°C with 1mN preloading condition and elongated in 50% strain/min speed, up to 500% of elongation. From tensile test, ultimate tensile strength, elongation at break, and 100% modulus of the samples were derived and compared

Samples at each phase, powder, porous structure, and infiltrated samples were observed with Nova 230 SEM (FEI, Hillsboro, Oregon) to check the surface characteristic, shape, and integration with structure. Powders, green parts, and infiltrated parts were observed. Each of the solid samples were sliced to razor blade(Fisher Scientific, Pittsburgh, Pennsylvania) to 1mm thickness and placed on to the SEM stage with carbon conductive tape. Powder samples were

gently placed on the carbon conductive tape on SEM stage and blew out excessive powder with compressed air blower. The samples were observed in Low Vacuum Detector, 50Pa Vacuum pressure, water vapor, and 3.0 spot size condition.

2.4. Result and Discussion

2.4.1. Ballistic Effect Characterization and Scanning Electron Microscopy on Powder

The designed binder has 26-43dyne/cm surface tension and 1-3cps viscosity which satisfy range of suggested surface tension and viscosity for minimal droplet deposition error with HP11 thermal inkjet [34]. Inverse of Ohnesorge number, Z value are larger than 14, except the PAA 16% binder and acetone based binder, and it showed the possibility of satellite droplet [33].

No significant difference depending on viscosity of binder was observed on Fig.2-3 and, viscosity of the binder solution may not affect on the ballistic effect at viscosity range for HP11 Printhead. Inertia force was assumed as dominant factor to ballistic effect due to low viscosity of the solution. Also, acetone-based binder had large ballistic effect on original silica treated silicone powder, compare to other PAA binder. High contents of low vapor pressure solvent in acetone based binder may leaded to because the bubble generation inside of thermal inkjet is largely affected by vapor pressure of the ink solution [35]. Polymer coating on silica treated silicone powder gave successful fixation to minimize ballistic effect as suggested on Fig.2-3. Fixation of the powder by moisture or polymeric coating has been suggested [36]. PVA and PVB coating on silica treated silicone powder showed fixation due to hydrogen bonding between hydroxyl functional group. Surface characteristic and polymer coating was observed with SEM. Original silica treated silicone powder showed low aggregation due to low attraction force contrary to polymer coated powders.

PVA coating did not showed even distribution on the surface of silica coated silicone powder and, silica treated silicone powder were not possible to have high hydrophilicity to hold PVA on the surface. Isolated chunk of PVA was also observed on Fig.2-5. PVB coating was cover surface of the powder more evenly.

2.4.2. Green Strength of Porous Structure and Scanning Electron Microscopy (SEM)

In printed samples with PVA and PVB coated powder, statistically significant positive relation between polymer coating ratio and 40% compressive modulus was observed, as indicated at Fig.2-6. PVA sample showed low compressive modulus compare to that of PVB. It is assumed unevenly distributed polymeric coating of PVA on the powder weaken the rigidity of the green parts as shown on Fig. On the other hand, more uniformly covered PVB require more energy to delaminate or fracture and result in increase in green strength. All of the samples were successfully formed porous structure based on connection by polymer between silica treated silicone powder. SEM observation on powder samples suggests thicker connecting area on PVB 7.0% compare to PVA7.0% in Fig.2-7. Thus, hydrophilic polymer coating and binder system allowed formation of porous green structure.

2.4.3. Mechanical Property of Infiltrated Structure and Scanning Electron Microscopy (SEM)

The rectangular porous structure was printed and infiltrated with silicone resin to confirm validity of silicone infiltration process as shown on Fig.2-8 Statistically significant positive relation between polymer coating ratio, 100% tensile modulus, tensile strength, and elongation at break were observed. It is assumed that increase in polymer ratio reinforce the connection between powder and make crack hard to propagate at interface. Also, the elongation at break shows 60% higher elongation at break than reported value in starch-silicone composite for PVB 7% sample [22].The 100% tensile modulus for PVA 7%, PVB 4.8%, and PVB 7% satisfied

0.35Mpa-1.7Mpa of moderated elastic modulus condition [37] required to move along with facial muscles movement. In SEM images, the crack and void generation on PVA samples were confirmed on SEM imgages, Fig2-10. PVB samples also possessed the void, but minor in size compare to PVA samples. It is assumed lipophobicity and low green strength of PVA sample. Forced infiltration generated crack on low density porous parts [38], and lipophobic surface characteristic of PVA was hindered wetting of the porous structure. Vinyl butyral functional group of PVB helped integration of lipophilic silicone and prevention of crack propagation at local area, and the interface was not delaminated until silicone failed.

The binder jetting approach with silica treated shows possibility in 3D printing of silicone with 322% elongation at break, even more than the 244% for starch infused samples [39]. It would be possible to increase ductility of 3D printed parts by enhancing integration at interface of powder-polymer-silicone. Wet and dry silane surface treatment were suggested to help the adhesion of silicone resin [40], and polymers on glass substrates [41]. Also, elastic modulus of the can be adjusted by changing elastic modulus of infiltration material, to satisfy requirement for maxillofacial prostheses applications, because elastic modulus of the composite material is dependent on elastic modulus of inclusions [42]. For next step, testing with clinical trial to build complex structure and compatibility with current coloring and adhesive system for retention. Multi-color 3D printing with voxel level control is expected to possible to print as applied on other powder material [43] by adapting multi printhead printing.

2.5. Conclusion

In this step, hydrophilic polymer coated silica treated silicone by spray drying and compatible solvent based binder system showed possibility of silicone powder based 3D printing for maxillofacial prosthesis. PVB coated powder printed samples high, 322% of elongation at

break exceed the reported value for previous starch based silicone composites. Also, moderate tensile modulus was achieved for PVA 7%, PVB 4.8% and, PVB 7% samples. For the next steps, optimization powder system and clinically test for 3D printed maxillofacial prostheses would require. In addition, by adding additional printhead, full color 3D printed sample can be fabricated.

2.6. Figures

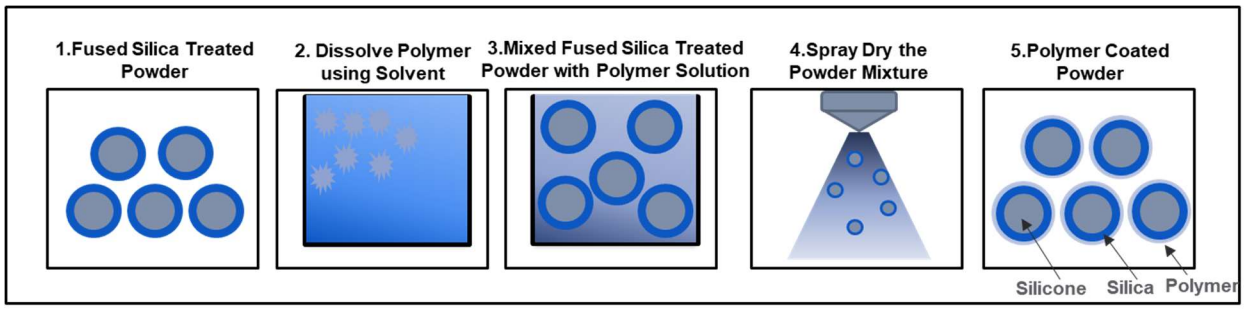

Figure 2-1. Schematic Diagram about Spray Drying procedure to coat silicone powder with polymer

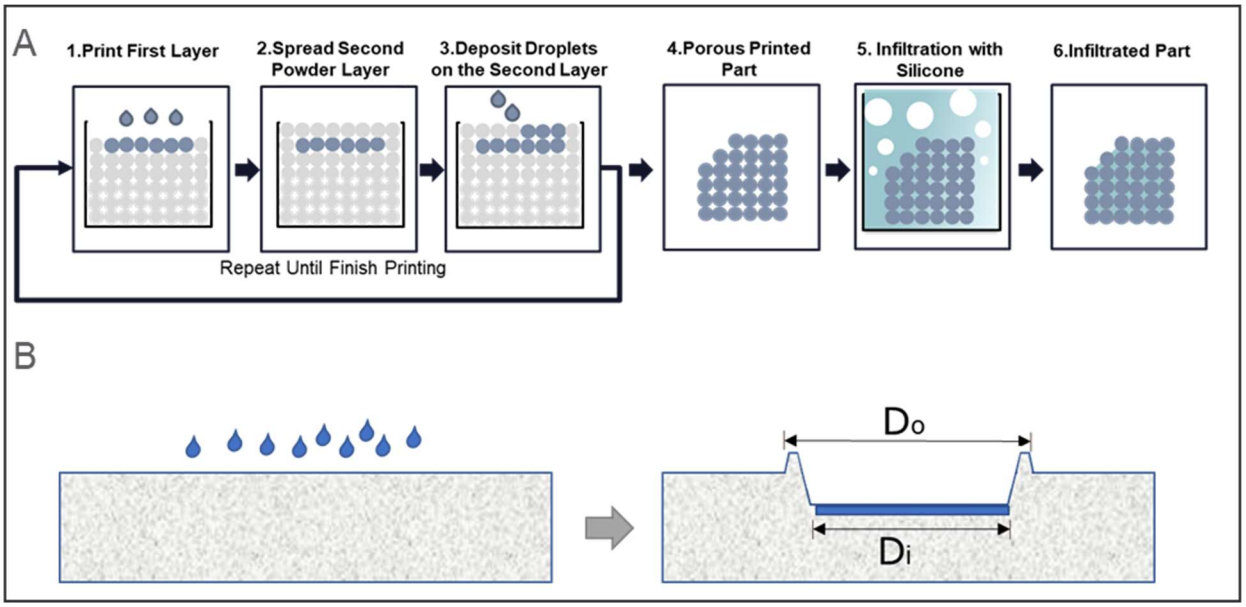

Figure 2-2. Schematic Diagram for Binder Jetting Approach (A) Binder Jetting Procedure and Infiltration for 3D printing (B) Crater generation during printing by Droplet deposition and Ballistic Effect.

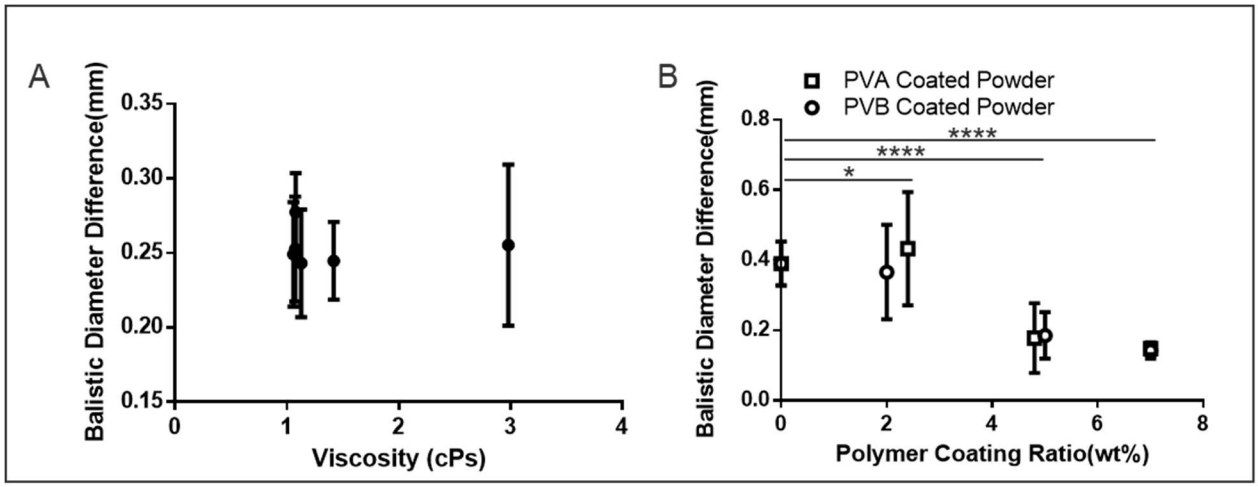

Figure 2-3. Ballistic Diameter Difference: (**A**) Ballistic Diameter difference depending on PAA binder solution viscosity; (**B**) Ballistic Diameter difference depending on polymer coating ratio with Acetone Based Binder. Asterisks denote statistical significance ((* denotes $p < 0.1$; **** denotes $p < 0.0001$;).

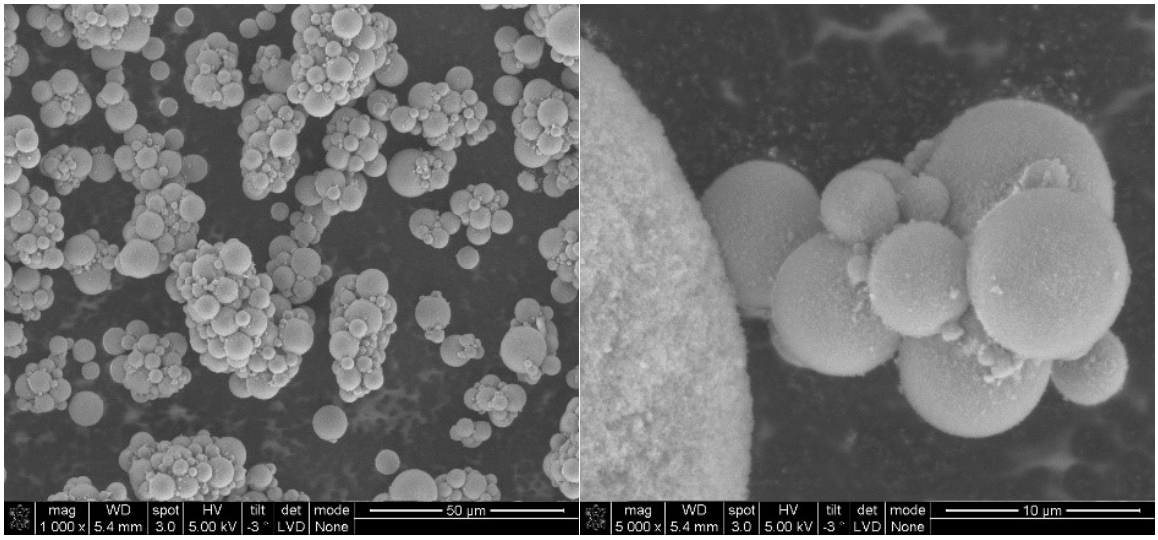

Figure 2-4. SEM image of Silica treated Silicone powder without polymer coating.

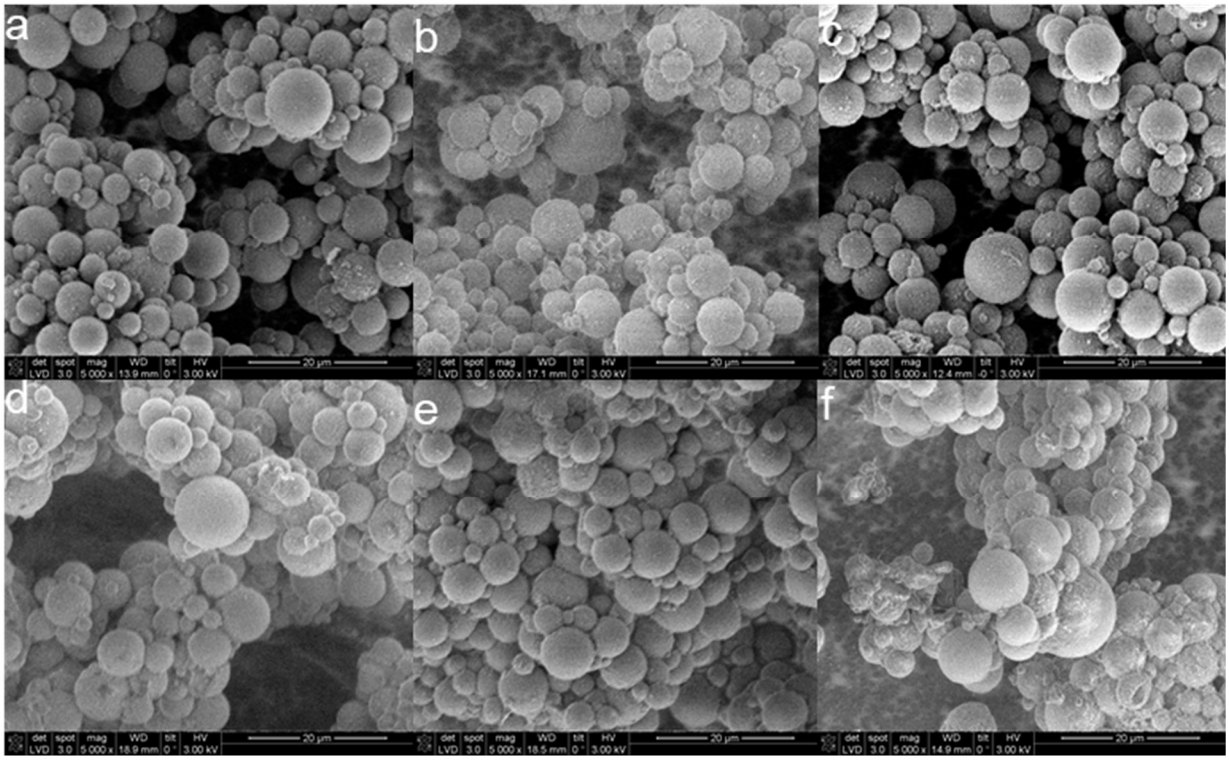

Figure 2-5. SEM image of Polymer coated silica treated silicone powder: (a) 2wt% of PVA coating (b) 5wt% of PVA coating (c) 7wt% of PVA coating; (d) 2.4wt% of PVB coating (e) 4.8wt% of PVB coating (f) 7.0wt% of PVB coating

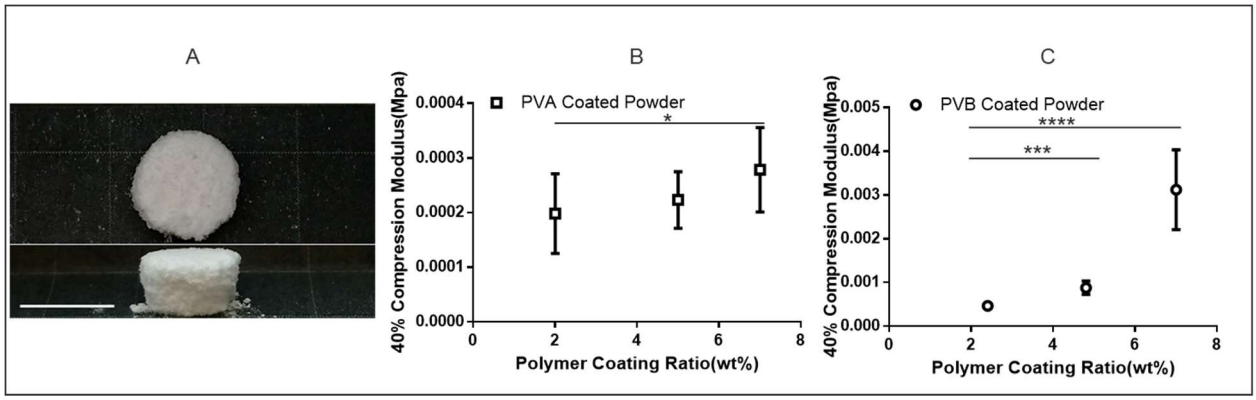

Figure 2-6. 40% Compressive Modulus Testing on Cylindrical Printed Samples: (A) Cylindrical Shape Sample with 10mm scale. (B) 40% Compressional Modulus of PVA coated powder printed samples. (C) 40% Compressional Modulus of PVB coated powder printed samples. Asterisks denote statistical significance ((* denotes $p < 0.1$; *** denotes $p < 0.001$;); **** denotes $p < 0.0001$;).

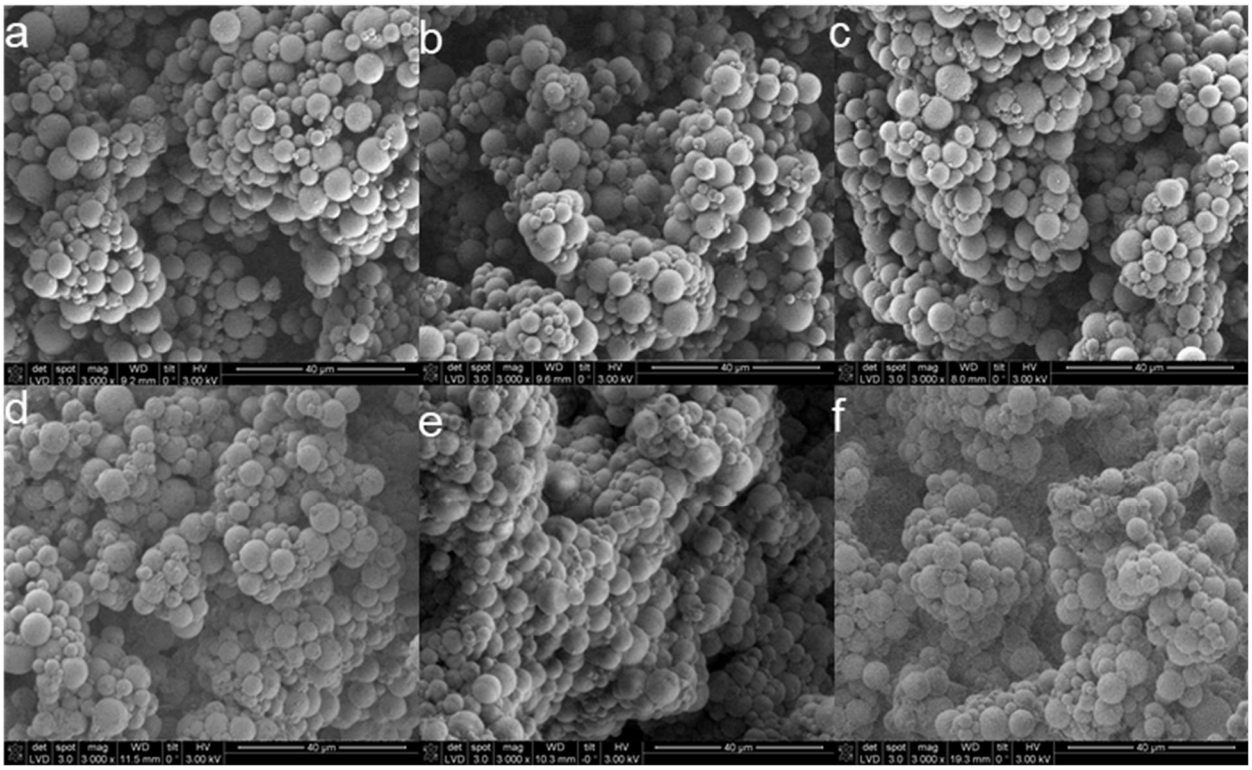

Figure 2-7. SEM image of Printed Porous Structure with Polymer coated silica treated silicone powder: (a) 2wt% of PVA coating (b) 5wt% of PVA coating (c) 7wt% of PVA coating; (d) 2.4wt% of PVB coating (e) 4.8wt% of PVB coating (f) 7.0wt% of PVB coating

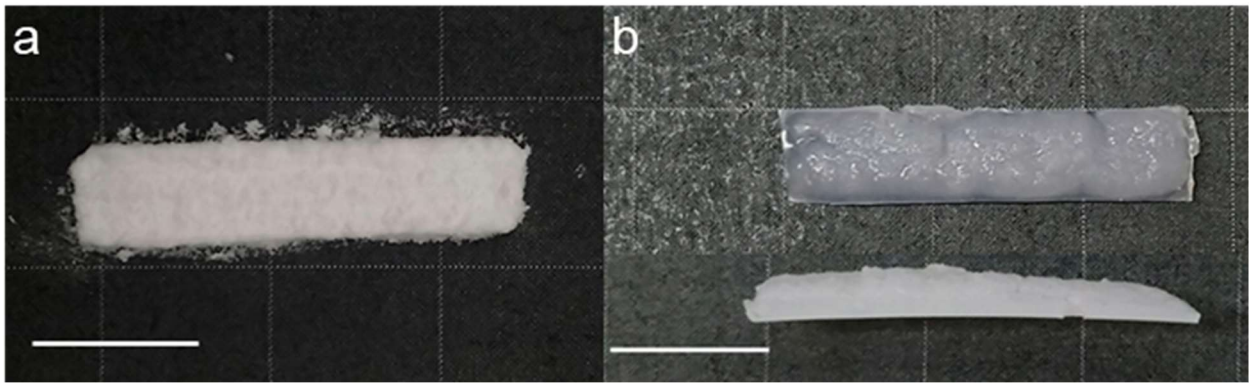

Figure 2-8. Rectangular Sample for Silicone Infiltration and Mechanical Testing (a) Rectangular Sample Before Infiltration (b) Rectangular Sample After Infiltration

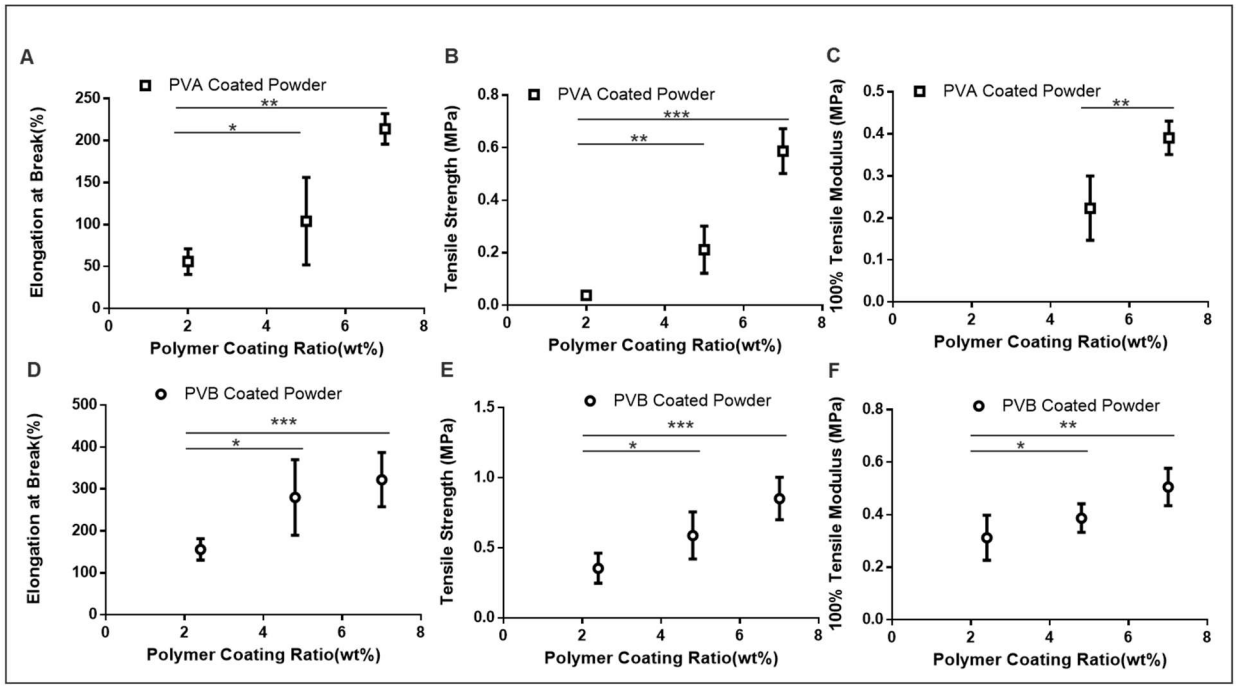

Figure 2-9. Tensile Testing about Silicone Infiltrated parts: (A) Elongation at Break of PVA coated Powder Samples (B) Tensile Strength of PVA coated Powder Samples (C) 100% Tensile Modulus of PVA coated Powder Samples. Note that PVA 2% samples were broken before 100% of elongation; (D) Elongation at Break of PVB coated Powder Samples (E) Tensile Strength of PVB coated Powder Samples (F) 100% Tensile Modulus of PVB coated Powder Samples

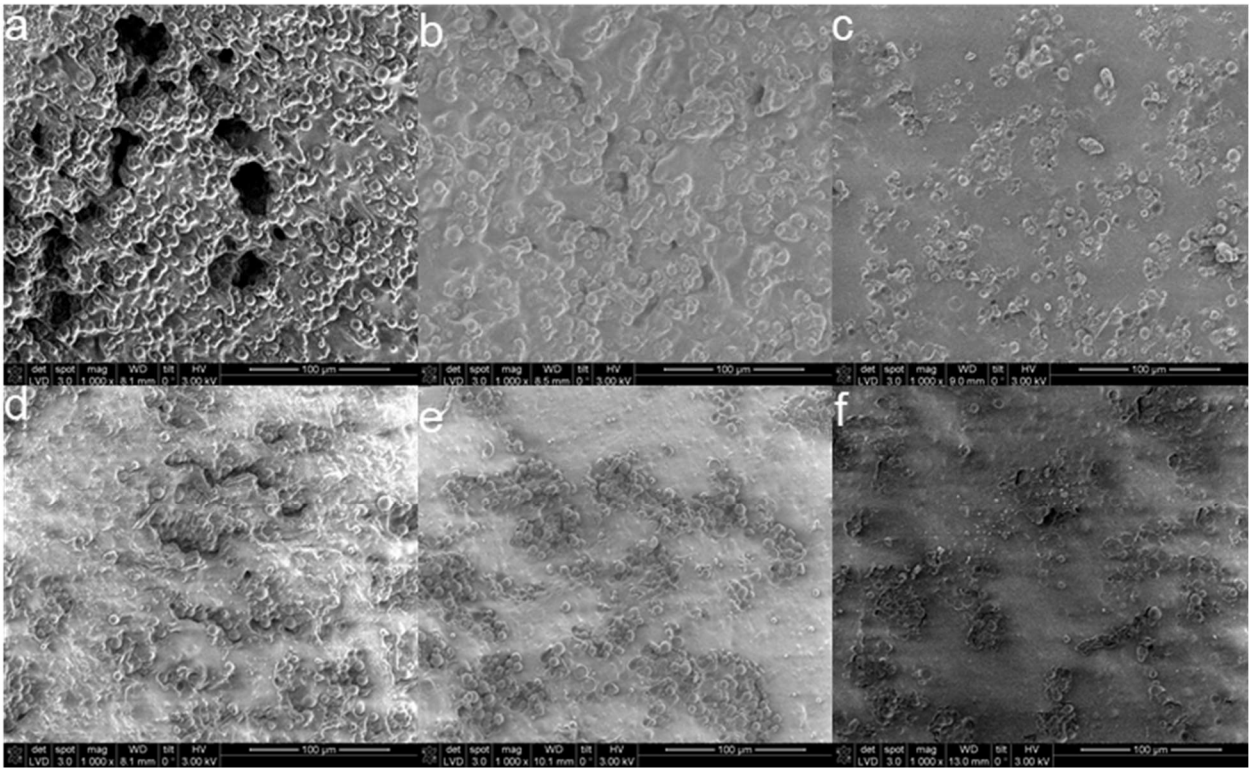

Figure 2-10. SEM samples about Silicone Infiltrated parts: (a) Elongation at Break of PVA coated Powder Samples (b) Tensile Strength of PVA coated Powder Samples (c) 100% Tensile Modulus of PVA coated Powder Samples; (d) Elongation at Break of PVB coated Powder Samples (e) Tensile Strength of PVB coated Powder Samples (f) 100% Tensile Modulus of PVB coated Powder Samples

2.7. Tables

Table 2-1. Composition of Silicone Powder mixture for Spray Drying

PVA coated Powder Fomulation	Polymer Coating Ratio(wt%)	Silica Treated Silicone Powder	PVA	Tween80	
	2.0%	19.6%	0.4%	0.25%	
	5.0%	19.0%	1.0%		
	7.0%	18.6%	1.4%		
PVB coated Powder Fomulation	Polymer Coating Ratio(wt%)	Silica Treated Silicone Powder	PVB	Ethanol	Acetone
	2.4%	20.0%	0.5%	50.0%	20.0%
	4.8%	20.0%	1.0%		
	7.0%	20.0%	1.5%		

Chapter 3. Control of Polymer Coated Silicone Powder Binder Jetting Material System

3.1. Abstract

In this study, morphology and size of polymer encapsulated silica treated silicone powder was successfully controlled by Ohnesorge number based approach on spray drying. Properly encapsulated silicone powder with poly vinyl butyral was used for 3D printing, and the printed green parts shows highly complex detail required for maxillofacial prostheses. Followed pressure-vacuum sequential silicone infiltration with silicone resin successfully transformed porous structure to highly flexible structure with moderate elastic modulus. In clinical testing, the printed ear prosthesis proved complex detail and contour matching requirement as maxillofacial prostheses. Even more, the printed prosthesis was compatible with medical adhesive for retention and silicone colorant. Thus, this study validity of silicone powder jetting approach to 3D print silicone maxillofacial prostheses and compatibility with adhesive retention and silicone colorant system for silicone maxillofacial prostheses.

3.2. Introduction

In previous step about compatible material system for silicone powder, PVB with silica treated silicone powder showed best mechanical property. To optimize its mechanical property in printed parts and infiltrated parts, dedicated control about particle size for silica treated silicone powder was required. Spray drying particles morphology and characteristic was suggested as function of Ohnesorge number, Oh which reflects the physical properties of the fluid droplet and atomization is derived from surface tension γ, viscosity μ, density ρ, and the nozzle outlet radius d in **Equation 1** [33].

$$Oh = \frac{\mu}{\sqrt{\rho\gamma d}} \quad (1)$$

Reynolds number, *Re* which reflects the physical properties of the atomized jet is derived from jet speed U, viscosity μ, density ρ, and the nozzle outlet radius d in **Equation 2** [33].

$$Re = \frac{\rho U d}{\mu} \quad (2)$$

To form stable droplet with spray-drying, these two non-dimensional number should be large enough to affiliated to atomization region [44]. For spray-drying jet in atomized region, droplet size can be controlled by Ohnesorge number. Volume mean diameter of atomized droplet size based on non-dimensional parameter has been suggested as **Equation 3** [45].

$$D_{vm} = C_1 C_d^{-\frac{2}{3}} \left(\frac{FR}{01}\right)^{\frac{1}{3}} * \left(\frac{P}{1bar}\right)^{-\frac{1}{3}} \left(\frac{\gamma}{\gamma_{H2O}}\right)^{\frac{1}{3}} \left(\frac{\theta}{110°}\right)^{-\frac{2}{3}} f_1(Oh) \quad (3)$$

C_1 and C_d is characteristic coefficient of spray dryer, *FR* is Froude number describing speed-length ratio of jet, P is pressure, γ_{H2O} is surface tension of water, θ is spray drying angle, and f_1, the characteristic function is defined for each of material. Even though this equation does not directly indicate the exact size of spray-dried powder but suggests the possibility of control of particle size of powder based on Ohnesorge number. In study about binder jetting approach, 31 microns median particle size condition showed balance between good packing density and surface roughness for green parts [46]. Thus particle size required to be controlled in 20-40 microns range, and the properties of printed parts and infiltrated parts were checked.

3.3. Material and Methods

3.3.1. Ohnesorge Number Based Control for Spray Drying of Silicone Powder

The amorphous fumed silica treated bis-vinyl dimethicone/dimethicone copolymer powder with 2μm average diameter, 3-7wt% silica ratio, and 1.01g/cm3 density was used for the main powder material. Silica treated silicone powder was surface treated with 3-Aminopropyl(diethoxy)methylsilane (Sigma-Aldrich) because amino-silane treatment promotes hydrogen bonding between Poly Vinyl Butyral and silica surface [47]. Silica treated silicone powder was dispensed in 60g of weight placed on polystyrene weighing dish (Fisher Chemical). Silane solution of 97 wt% ethanol, 1 wt % DI water, 2 wt % silane was vortexed and left for an hour for hydrolysis. The weighing dish with silicone powder was placed on tempered glass container and 2g silane solution was poured directly on the glass container without direct contact with the silicone powder. The glass container was closed and purged with nitrogen to prevent unwanted reaction with oxygen. Then the glass container was placed in incubator in 40 °C, 24hour condition to help formation of silane vapor and reaction with silica surface. To compare the effect of silanization on mechanical property and air volume of printed parts, one control group without silane surface treatment was prepared.

The PVB powder solution was formulated by dissolving Butvar®-76 and Butvar®-98(Sigma-Aldrich) in mixture of DI water and Reagent Alcohol (Fisher Chemical) via closed flask in an 60 °C water bath for 30 min. After complete dissolution, the mixture was removed from heat and silica-treated silicone powder was then distributed into the mixture using a magnetic stir bar and plate for approximately 20 min. The final mixture was stored in a closed poly bottle at room temperature until further use.

To confirm effect of Ohnesorge number on PVB and organic solvent material system, four different spray drying mixture with 5%, 12.5%, 16%, and 20% non-volatile contents ratio with fixed PVB 16% polymeric coating ratio. To compare effect of polymeric coating ratio, samples with fixed non-volatile ratio of 12.5%, and controlled PVB ratio with 8%, 12%, 16%, and 20% were tested. Composition, fluid mechanical properties of spray drying mixture are on table b. Spraydrying mixture satisfies the Reynolds number and Ohnesorge number requirement as shown on Fig. 3-1.

The spray drying of the powder mixtures were performed using a Mini Spray Dryer B-191 and a 1.45mm-sized nozzle. The aqueous powder mixture was fed to the droplet atomizer using a length of tubing through a circulating peristaltic pump. Droplets of solution are sprayed through the nozzle into the drying chamber, where the moisture is removed to leave solid particulate. The resultant powders are collected via cyclone and deposited into the collection vessel, where the final powder can be removed for use. Stiff, polyethylene sheets are used to remove excess powders adhered to the interior walls of the drying and cyclone chambers. In instances of excessive powder adhesion to the borosilicate chambers, the collected powders are further filtered twice using a 500μm and 100μm sieve to restrict the powder particle size prior to use. The standard preset condition was used for the PVB powder mixture, which maintained the inlet temperature, sample feed rate, and compressed air flow rate at 65 °C, 20%, 600 L/hour, respectively at 90% vacuum aspiration.

Also, we tested if addition of PVB on spray dried powder can increase the green strength of the material. B98 powder was filtered with 100-micron filter and mixed with PVB16% non-volatile ratio 12.5% silicone powder in 1:4 ratio on the test group

The viscosity of spray drying mixture was measured in a rheometer (Discovery HR-2, TA Instruments) with a 40 mm 2.016◦ plate attachment and shear rate ranging from 25 to 630 Hz in shear sweep method. Average viscosity at 100 Hz data was used to compare the viscosity. The surface tension was measured with Ds/De pendant-drop method with the FTA125 goniometer (First Ten Angstroms, Portsmouth, Virginia) and calculated based on image processing on ImageJ.

3.3.2. 3D printing of Porous Structure and Characterization

The base 3D printing binder formulations used for 3D printing consisted of acetone(15 wt%) (Fisher Chemical), HPLC grade ethanol(30 wt%) (Sigma-Aldrich), Isopropyl alcohol(15 wt%) (Sigma-Aldrich), DeIonized water(28.9 wt%) , and Polyvinylpyrrolidone with M.W 10000 (1 wt%) (Sigma-Aldrich). FD&C Red #40 powder pigment (0.1 wt%) (ColorCon) and were added to the base solution. The solutions were prepared in 40 g with a 50 ml conical tube and vortexed for 1 min, or until homogenous as needed. Excess particles were filtered from the binder solutions using a 0.2 microns Polytetrafluoroethylene filter (Fisher Chemical) before loading of the binder into the printhead cartridges for use.

To print parts with binder jetting approach, Z510 printer was utilized. First, build and feed platform of Z510 printer were lowered to avoid interference. Then prepared printheads were installed on the fast axis assembly. The powder was set on the feed piston. Then the powder was packed using flat acrylic plate. The powder was spread by the roller in fast axis and repeating built in spreading function. 0.1mm layer thickness and 21.7% uniform binder saturation with monochromatic binder option was used for 3D printing. To build designed parts, the printer spread a single layer of powder and deposited solvent based binder to dissolve coating on the powder which leaded to connection between powder. This process was repeated until the last layer of porous printed part was printed. The printed parts were dried in the 3D printer for 24 hours to

prevent crack or warping. The powder encapsulating parts was carefully removed in the post processing unit of Z510 printer with air gun in 5kPa pressure and brush. For green strength testing, 10Φx5t (mm) cylindrical shape samples were prepared for each of powder groups. For tensile testing, 25Lx5wx1t (mm) rectangular bar shape samples were prepared. Green Strength test was conducted in same procedure for mechanical test samples on chapter 2.3.3

Air Volume in disc samples were observed with Micro CT scanning and reconstruction to 3D. The cylindrical samples were measured by Skyscan1176 Micro CT (Bruker micro-CT, Kontich, Belgium) with No filter, 900 ms exposure time, 40 kV Voltage, 0.40° step angle, 4000 x 2672 resolution, and 9 micron per pixel size condition. After measurement, the sample was reconstructed to 2D cross sectional bitmap images with Nrecon (Micro Photonics Inc., Allentown, Pennsylvania), and reconstructed to 3D model with Mimics (Materialise, Leuven, Belgium). Then air volume of 3D reconstructed model in 8Φx4t(mm) disc shaped control volume was calculated with boolean function.

3.3.3. Silicone Infiltration of Porous Structure and Characterization

The cleaned parts for tensile testing samples were infiltrated with silicone resins, to make them to full dense parts. The two parts 20A hardness platinum cure silicone, RTV 4420(Bluestar Silicones USA Corp), and HexaMethylDiSiloxane (HMDS) solvent, Novocs Gloss (Smooth-On, Inc.) were dispensed to conical tube in 75%, and 25% ratio by weight. The ratio between part A and B of RTV 4420 was kept in 1:1 for all of test condition. The conical tube was vortexed for 1 minutes to evenly mix the contents. Forced wetting condition was applied in 3 bar pressure condition with compressed air in zinc plated pressurized tank (McMaster-Carr) for 30 minutes. After 30 minutes, we release the compressed air slowly, below 3bar/minutes rate pressure change to prevent possible stress generation. The chamber was connected to vacuum with -0.7 Bar

pressure to further increase infiltrated area and remove the solvent. After 30 minutes, the release valve of the chamber was slowly opened to recover the pressure of chamber to atmosphere pressure, below 3bar/minutes rate. To check the effect of HMDS, one extra group was printed with additional B-98 condition and infiltrated silicone resin with 35% HMDS ratio and 65% RTV4420. Tensile test was conducted in same procedure for mechanical test samples on chapter 2.3.3

3.3.4. Proof of Concept Testing for Ear prostheses and clinical trial.

A male patient from the University of California at Los Angeles maxillofacial prosthetics clinic was selected and agreed to participate in the proof of concept evaluation of the adhesive-retained 3D-printed ear prosthesis. The patient was scanned with Artec Eva-M 3D scanner (Artec 3D, Palo Alto, California). During scanning, geometry and color texture of the patient were scanned simultaneously. Then, scanned data was merged together and texture mapping with the Artec Studio (Artec 3D). The scanned data was processed with Zbrush (Pixologic, Los Angeles, California) to construct ear prostheses match with contour of the defect. Then printed in monochromatic model with Z510 3D printer with PVB16%, 12.5% nonvolatile ratio mixed with 20% B98, and infiltrated with RTV4420 resin mixed with HMDS in 35% by weight. Initial try-in with the printed prostheses was attached on the volunteer with DARO medical adhesive (Factor II, Lakeside, Arizona), and FE-Extrinsic Colors (Factor II) that contain FD&C cosmetic pigments into a silicone crosslinking fluid and the silicone-containing FE-100 solvent (Factor II) was treated over the surface of prostheses to confirm availability of the traditional paint technic on 3D printed prostheses.

3.3.5. Scanning Electron Microcopy about particle, porous structure, and infiltrated samples.

Samples was observed with Nova 230 SEM to characterize spray dried powder and printed parts. Particle size and aspect ratio of spray dried powder was measured on 500x scale image from

SEM with ImageJ. The surface characteristic, shape, and integration with structure on green parts, infiltrated parts, and fractured cross sectional area after tensile testing were observed. Each of the solid samples were sliced to razor blade (Fisher Scientific) to 1mm thickness and placed on to the SEM stage with carbon conductive tape. Powder samples were gently placed on the carbon conductive tape on SEM stage and blew out excessive powder with compressed air blower. The samples were observed in Low Vacuum Detector, 50Pa Vacuum pressure, and water vapor condition

3.4. Result and Discussion

3.4.1. Characterization of Spray Dried Particles

Fixed 16% polymer coating ratio with 5%, 12.5%, 16%, and 20% polymer coating ratio and fixed 12.5% non volatile ratio with 8%, 12%, and 20% polymer coating ratio samples were spray dried and observed particles with SEM. Particle size and morphology on SEM images for spray-dried powder were analyzed with ImageJ. All samples were satisfying atomization condition suggested on spray drying model [44], as shown on Fig. 3-1.

Change of the particle size, aspect ratio showed significantly positive relation with Ohnesorge numbers, as marked on Fig. 3-2. As SEM image of non-volatile ratio 20% sample indicates, excessively large particle can be easily formed at high Ohnesorge number condition for spray-drying condition as the formation of large size atomized droplet before drying of powder, and agglomeration on dried powder on Fig. 3-3. Polymer Coating ratio control group showed less dramatic change in particle size and texture compare to non-volatile ratio group, which may suggest possibility of dual control of polymer coating ratio and Ohnesorge number to optimize powder size and morphology for powder based 3D printing. Except non-volatile ratio 5% and 20% group and polymer coating ratio 8% group, median of particle size were between 20 to 40 microns.

Even though non amino silane treated group and amino silane treated group did not showed significant difference in Ohnesorge number but showed significant difference in particle size, which may suggest damage, separation, or improper encapsulation polymer coating without proper silane treatment, due to low bonding strength.

3.4.2. Property of Porous Structure and Scanning Electron Microscopy (SEM)

Non volatile ratio control, polymer coating ratio control, and additive control group were printed in cylindrical shape and tested for 40% compressional modulus, and air volume in control volume as shown on Fig. 3-4. In SEM images on Fig. 3-5, all samples showed porous structure formation by binder jetting technic with organic solvent-based binder. The formed porous structure showed interconnection between silica treated silicone powder by PVB. Increase in PVB can improve green strength but involves increase in air-volume between particle as shown on polymer coating ratio 20% samples. By decreasing non-volatile ratio, we could decrease air volume to allow tight packing of particles, but 12.5% non volatile ratio samples shows maximum green strength rather than 5% non volatile ratio sample with lower air volume. This is because too low viscosity of spray drying mixture may result in failure in encapsulation of particle [48] and result in defect of porous structure. Addition of PVB on spray dried powder did not hinder green strength of 3D printed structure as shown on Fig. 3-4(F). Otherwise, non-silane treated samples shows highly noticeable decrease in green strength and increase in air volume compare to control group, which indicate importance of amino silane treatment to create strong enough green parts survive during post processing.

3.4.3. Mechanical Property of Infiltrated Structure and Scanning Electron Microscopy (SEM)

The porous green parts were infiltrated with silicone resin diluted by HDMS in 3 bar pressure and -0.7 bar vacuum condition. Non volatile ratio, polymer coating, and additive

condition control group were prepared in rectangular shape and tested in tensile mechanical properties on Fig.3-6. Among the infiltrated samples before applying tensile stress, no significant crack or damage were observed, and minor pores were observed on Fig. 3-7. All sample group showed elastic modulus between 0.39-0.46 MPa which satisfying similar elastic modulus compare to that of the skin. Ideal hardness for facial prostheses had been suggested as 25 to 55 A hardness [37]. Shore 30.3 A prosthetic silicone had 0.345 MPa, and shore 44.3 A hardness prosthetic silicone had 0.794 MPa of 100% modulus [49]. Thus, all sample group satisfied the ideal range of elastic modulus and hardness, because linear relation between hardness and elastic modulus on elastomeric silicone had been proven [50], and samples satisfied the elastic modulus condition.

Also, all sample groups had average elongation at break higher than 300%, and 5% non-volatile ratio sample showed the average elongation at break at 398%, which was about 4 times of that of Tangoplus [51]. Extra PVB B-98 with HMDS 35% group shows highest elongation at break with 440% of strain. Facial movement of muscle involves only 10% of deformation of prostheses, but it has been suggested that ideal facial prostheses require to have about 400-800% of elongation at break [37]and widely used commercial prostheses material MDX-4-4210 [52] showed 394.3% elongation at break [49]. Polymer coating ratio 8%, non volatile ratio 5%, non volatile ratio 16%, extra B-98 groups had elongation at break closes to ideal facial prostheses.

Positive relation between Polymer coating ratio and 100% elastic modulus was observed on samples. It is assumed that B-98 had 2.1-2.2 GPa and B-76 had 1.9-2.0 of elastic modulus [53], which are quite higher than that of silicone in composite, which suggest control of elastic modulus with polymer coating ratio. Tensile strength did not show statistically significant difference between samples, and polymer coating 8% and 16% samples shows 0.94 p-value between them, which may suggest increase in PVB would not lead to failure of infiltrated structure in constant

stress condition. Nevertheless, as increase of polymer coating ratio, little decrease in elongation at break was followed, this is because PVB had lower elongation at break of 100-120% [53] compare to that of RTV 4420 [54].

Non-volatile ratio had negative relation with tensile strength, elongation at break, which suggest increase in Ohnesorge number can result in failure of proper spray dried powder generation and result in relatively fragile silicone-silica-PVB-silicone composite matrix. Thus, it is required to control Ohnesorge number also for post-processed parts. Non-volatile ratio control on 100% elastic modulus showed statistically weak relation and control of elastic modulus by polymer coating ratio would be more effective for control of elastic modulus.

Additive conditions and silane treatment were tested on the infiltrated parts. Non-silane treated sample showed 0.1 Mpa decrease in tensile strength, but it was low changes compare to about 88% decrease in green strength. Thus, integration between silica treated silicone powder and PVB by amino silane treatment possibly affect on mechanical property of infiltrated parts, but other factors, such as integration between silicone resin and porous structure may be affected on mechanical property. B98 addition on amino silane treated powder showed 12% decrease in 100% modulus but did not showed significant change in elongation at break and tensile strength, which suggests that addition of polymer coating after spray drying may help to control mechanical property without lowering tensile strength and elongation at break on infiltrated parts. Not significant differences were observed for HMDS 25% condition and HMDS 35% condition in tensile modulus, but significant increase in tensile strength and elongation at break was observed as decrease in viscosity with help of HMDS [55].

3.4.4. 3D printed Ear Prosthesis Proof of Concept Test

To confirm the possibility of silicone powder 3D printing on maxillofacial application, proof of concept parts was printed and infiltrated with pressure and vacuum sequential process as shown on Fig.3-8 and Fig. 3-9. The prosthesis was attached with medical adhesive and showed tight contour matching with the trauma of volunteer and complex detail such as tragus, helix, and antihelix. The attached prosthesis was colored with touch-up coloring and showed well blended color with patient skin shade near the trauma. Thus, the possibility of flexible 3D printed material and structure can be matched with patient trauma, survived with overhang and thin edges and painted with current coloring system was proved.

The binder jetting approach with silica treated silicone powder shows possibility in 3D printing of silicone with 440% elongation at break, even more than the 244% for starch infused samples [22]. Silane surface treatment was successfully promoted adhesion of PVB on silica layers. For next steps, full color 3D printing with voxel level control is required by adapting multi printhead printing. The other aspect which should be considered in next step is weathering resistance, to guarantee life span in moisture and UV induced weathering condition

3.5. Conclusion

In this chapter, Ohnesorge number based approach was conducted to control spray drying of silica treated silicone powder encapsulated with PVB. Control of Ohnesorge number led to successful control on particle property combined with amino silane treatment. The PVB coated silicone powder with size control and organic solvent based binder allowed 3D printing of porous structure with complex detail by binder jetting. Followed pressure-vacuum sequential silicone infiltration with silicone resin successfully transformed porous structure to highly flexible structure with moderate elastic modulus. In clinical testing, proof of concept ear prosthesis was fabricated

and tested. The ear prosthesis proved validity of silicone powder jetting approach to 3D print silicone maxillofacial prostheses and compatibility with adhesive retention and silicone colorant system for silicone maxillofacial prostheses.

3.6. Figures

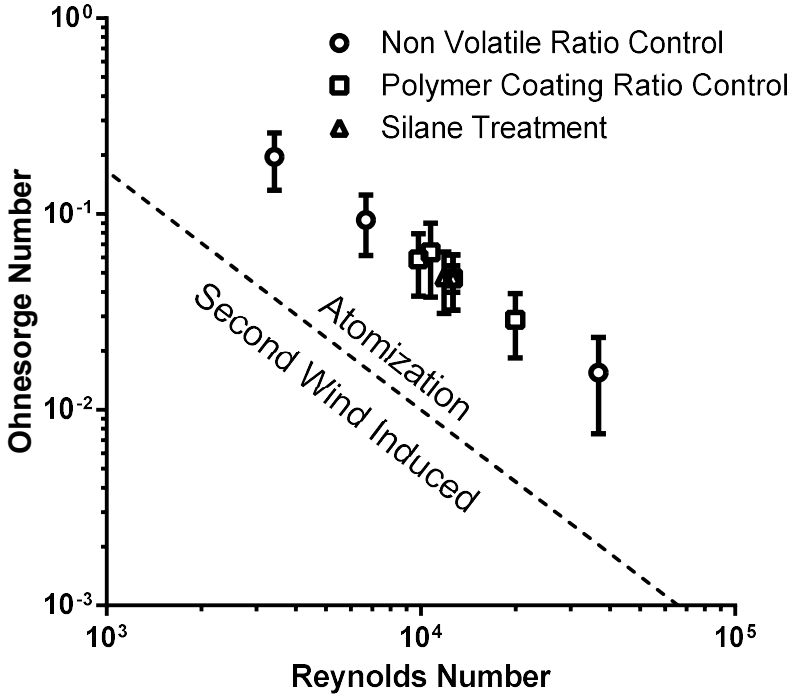

Figure 3-1. Reynolds Number and Ohneosrge Number dependent modes of spray drying and Non Dimensional Numbers for spray drying Samples.

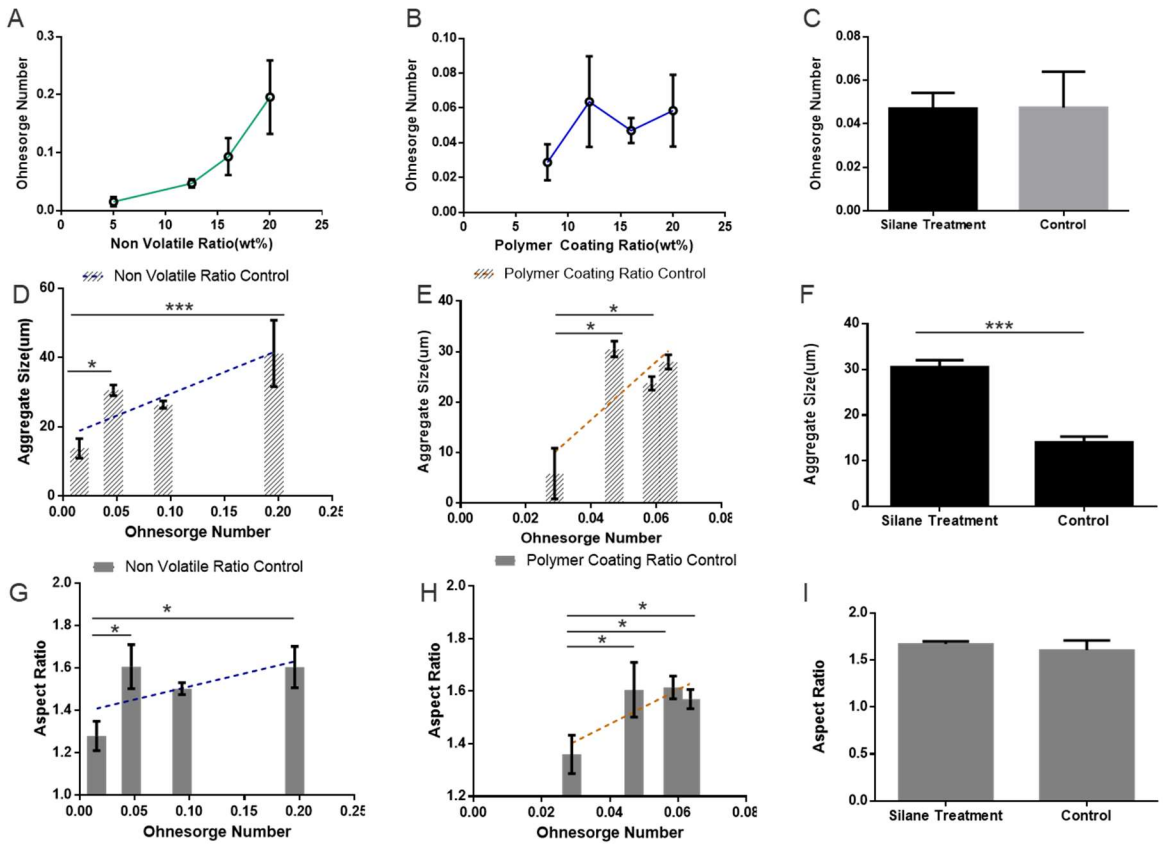

Figure 3-2 Ohnesorge Number, Particle Size, Morphology for spray Drying sample groups. (A-C) Ohnesorge number depending on Non volatile ratio control, Polymer coating control, and silane treatment. (D-F) Particle Size depending on Non volatile ratio control, Polymer coating control, and silane treatment. (G-I) Aspect Ratio depending on Non volatile ratio control, Polymer coating control, and silane treatment.

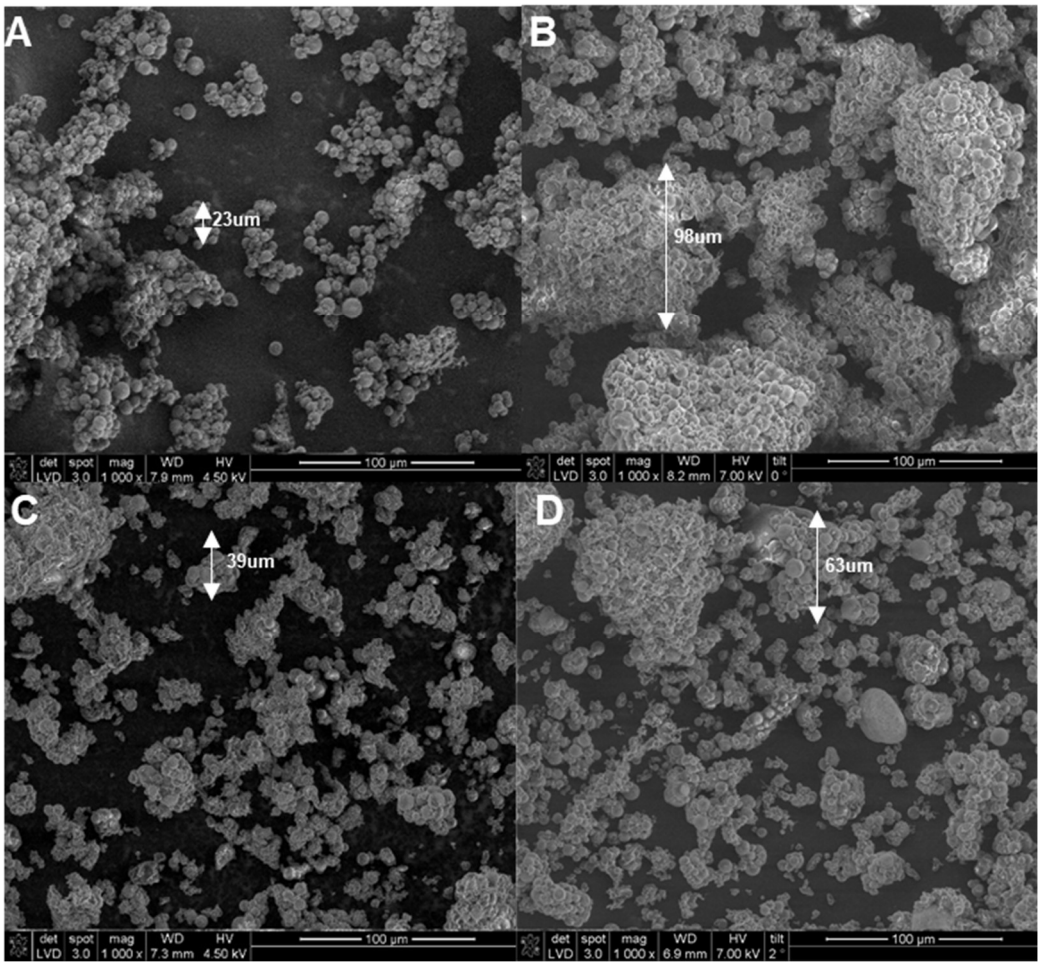

Figure 3-3. Scanning Electron Microscopy on Spray Dried Particles. (A) Non volatile ratio 5%. (B) Non volatile ratio 20%. (C) Polymer Coating ratio 8% (D) Polymer Coating ratio 20%

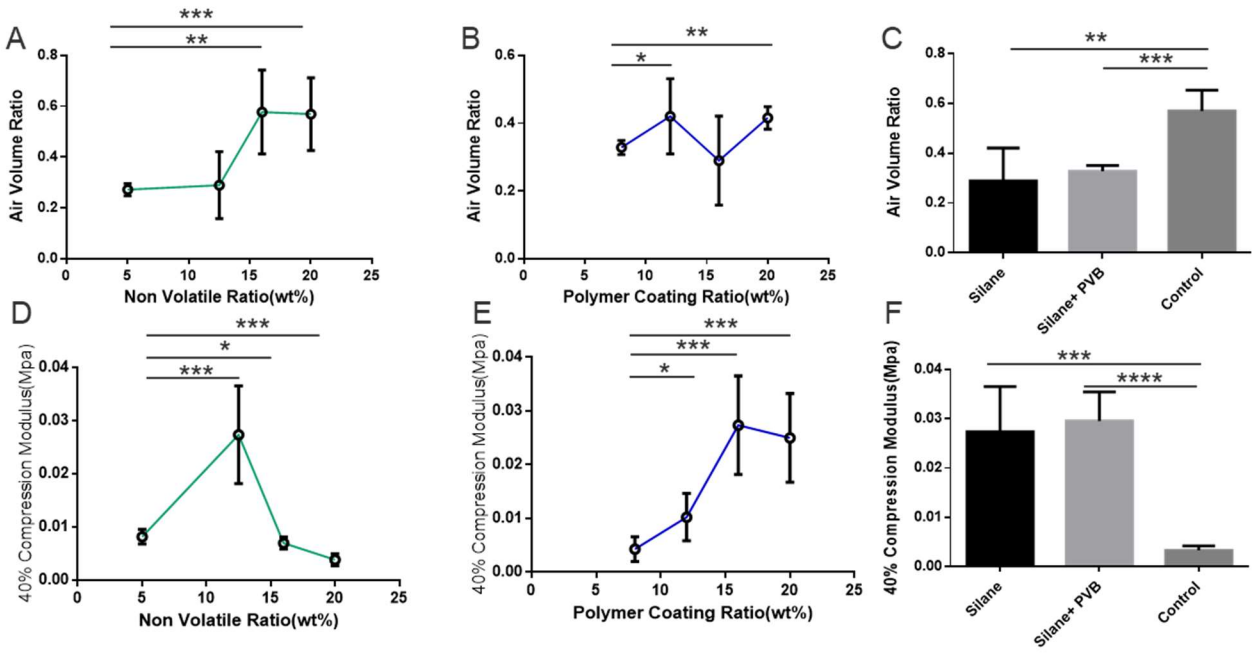

Figure 3-4. Air Volume and Green Strength for 3D Printed Porous Structure. (A-C) Captured Air Volume depending on Non volatile ratio control, Polymer coating control, Silane treatment, and additional PVB B-98. (D-F) Green Strength depending on Non volatile ratio control, Polymer coating control, Silane treatment, and additional PVB B-98.

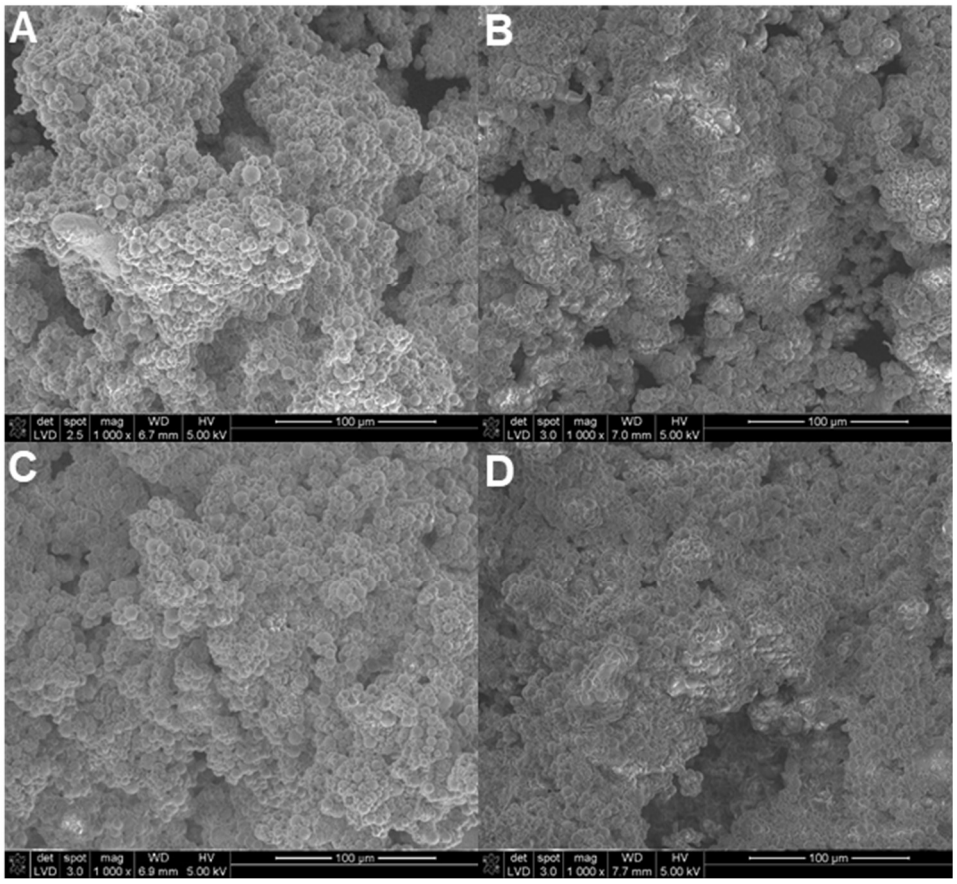

Figure 3-5. Scanning Electron Microscopy on 3D printed Porous Structure. (A) Non volatile ratio 5%. (B) Non volatile ratio 20%. (C) Polymer Coating ratio 8% (D) Polymer Coating ratio 20%

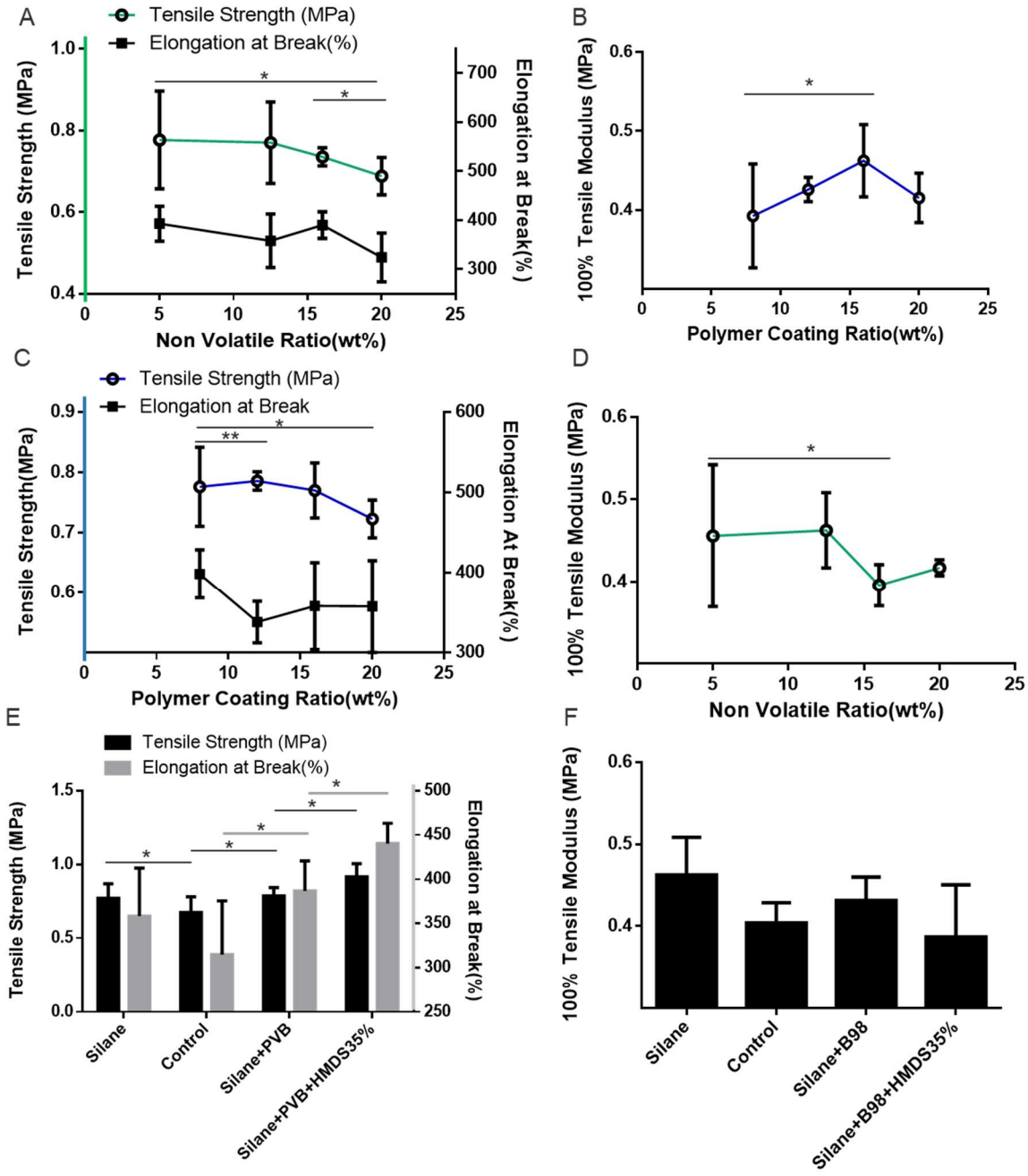

Figure 3-6. Mechanical Properties of Silicone Infiltrated Structure. (A-B) Mechanical Properties of Non volatile ratio control. (C-D) Mechanical Properties of Polymer Coating ratio control. (E-F) Mechanical Properties of Silane Treatment, Additional PVB, and HMDS ratio control.

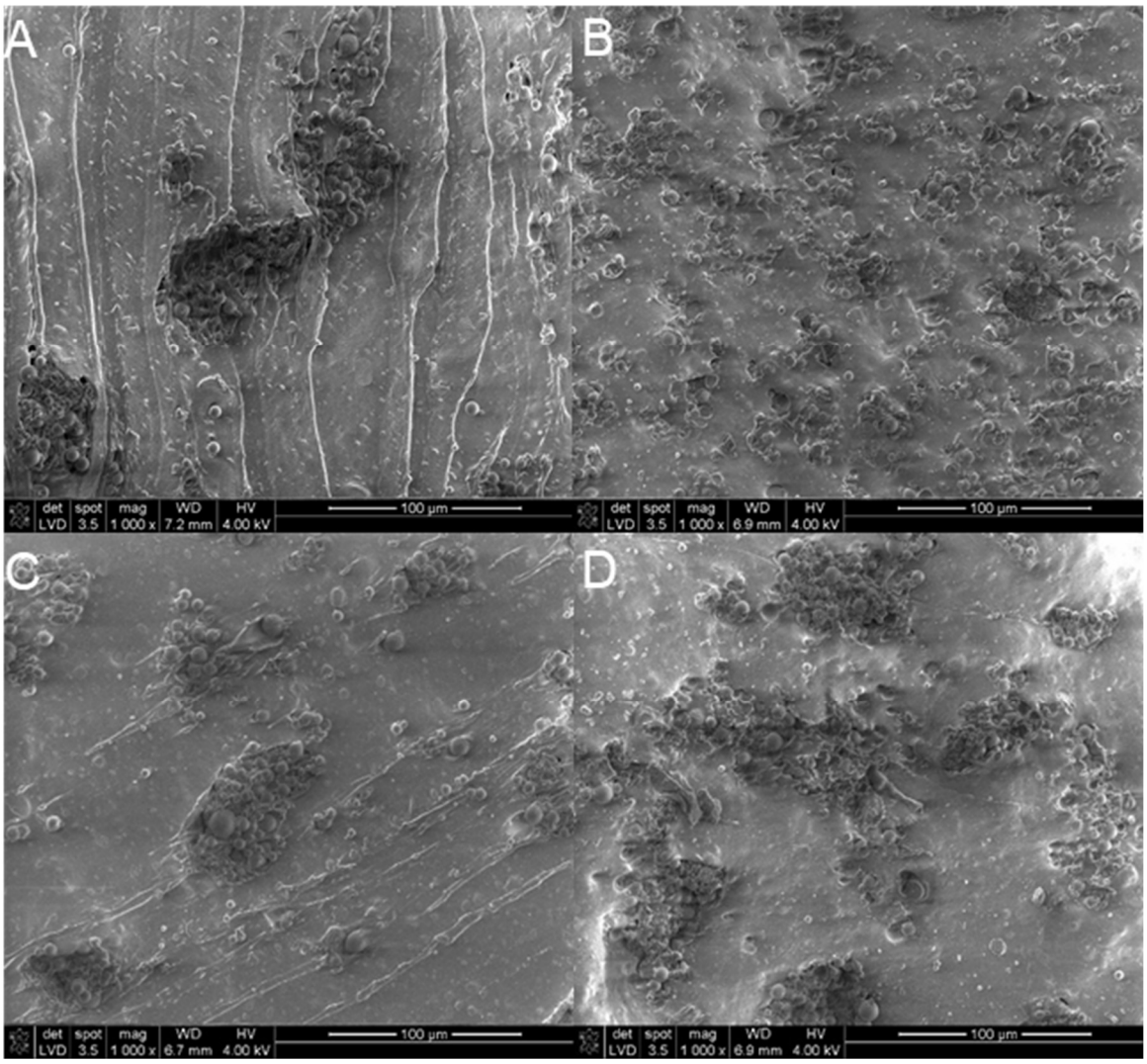

Figure 3-7. Scanning Electron Microscopy on Silicone Infiltrated Structure. (A) Non volatile ratio 5%. (B) Non volatile ratio 20%. (C) Polymer Coating ratio 8% (D) Polymer Coating ratio 20%

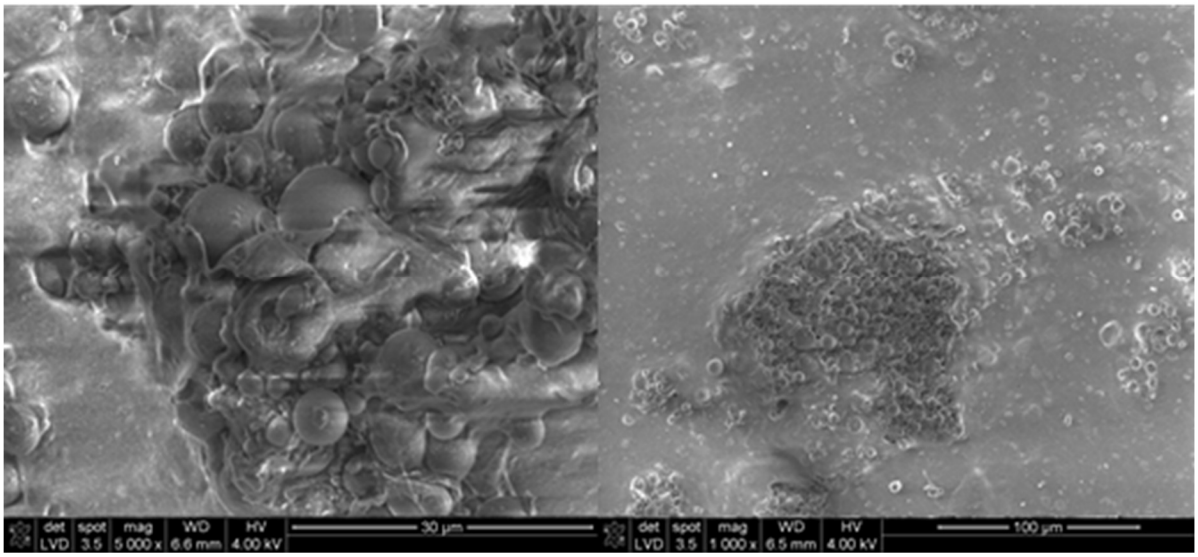

Figure 3-8. Scanning Electron Microscopy on Silicone Infiltrated Structure for Proof of Concept Ear Prosthesis.

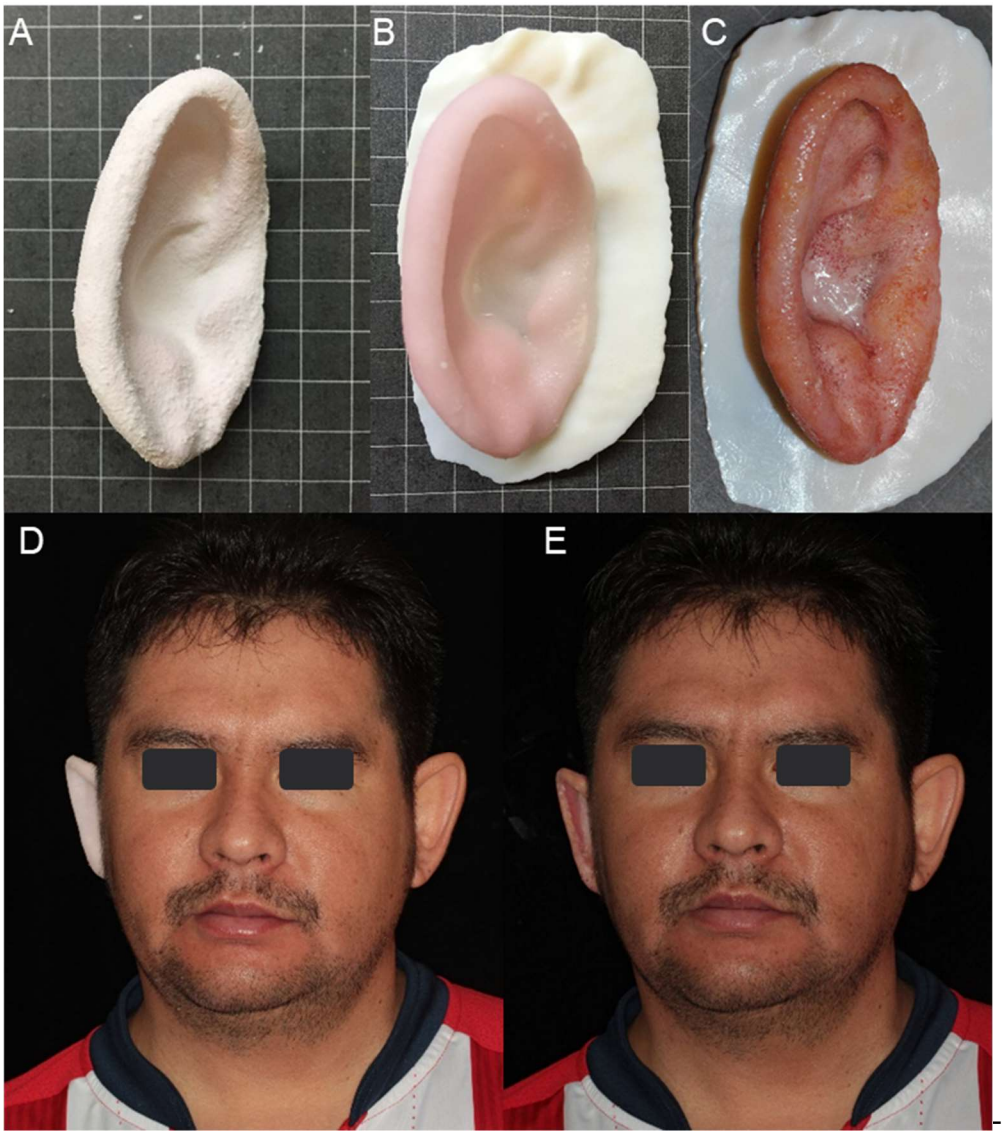

Figure 3-9.Proof of Concept Ear Prosthesis for Clinical Trial. (A) Printed Porous Structure for Prosthesis. (B) Silicone Infiltrated Prosthesis. (C) Manually painted Prosthesis. (D) Adhesive Retained Prosthesis on the Volunteer Patient. (E) Color Matched Ear Prosthesis with Patient Skin Shade.

3.7. Tables

Table 3-1. Composition of Silicone Powder mixture for Spray Drying for Ohnesorge Number based Control

Non Volatile Content Ratio	Ethanol	Water	SiO2 Treated Silicone	B-98	B-76
5.00%	85.00%	10.00%	4.38%	0.31%	0.31%
12.50%	77.50%	10.00%	10.94%	0.78%	0.78%
16.00%	74.00%	10.00%	14.00%	1.00%	1.00%
20.00%	70.00%	10.00%	17.50%	1.25%	1.25%
PVB Polymer Coating Ratio	**Ethanol**	**Water**	**SiO2 Treated Silicone**	**B-98**	**B-76**
8.00%	82.00%	10.00%	11.50%	0.50%	0.50%
12.00%	78.00%	10.00%	11.00%	0.75%	0.75%
16.00%	74.00%	10.00%	10.50%	1.00%	1.00%
20.00%	70.00%	10.00%	10.00%	1.25%	1.25%

Chapter 4. Full Color 3D printing and Weathering Resistance

4.1. Abstract

Cyan, magenta, and yellow pigments were engineered by surface treatment and wet ball milling for particle size reduction to submicron size in organic solvent binder system for silicone powder 3D printing. The engineered pigments were dispersed in organic solvent with enough stability by zeta potential control. The designed binder showed full color 3D printing availability in skin color printing and full colored ear prosthesis. Weathering resistance in ultraviolet radiation and moisture condition was proved for color and mechanical property, which guarantee enough life span for 3D printed maxillofacial prostheses. Thus, direct full color 3D printing of silicone was achieved, and printed parts were survived with enough life span in weathering condition.

4.2. Introduction

In printing of monotonous ear prostheses, the mechanical property and compatibility with current retention and color system was confirmed. By adapting multiple printhead with each of different color and applying them for 3D printing, full color 3D printing based on silicone powder can be achieved. Overall, two different color system was used to conduct full color 3D printing and characterize result. Cyan-Magenta-Yellow color system, three different color binder and clear binder was used to print full color parts. As subtractive characteristic of CMY [56], each of pigment absorbed light with selective wave length of light, as the colors are added, the printed parts looks darker. Colors were not mixed inside of printhead but were printed in tenth micron size of droplets on parts to make parts with full color. Each of dot called pixel for 2D, and in 3D they form cube called voxel [20].

To consist CMY color system, lake pigments were used for printing. Lake pigments have stability, biocompatible characteristic compare to dye, but they are ionic chemical and are

agglomerated easily by hydrogen bond formation [57] and low dispersibility at solvent based binder. Thus, surface modification with lipophilicity and hydrophobicity is highly required.

Lab, which is color system based on human perceptible color [58] was used. The major difference between Lab and other color system such as RGB is range of included color, and device dependence, and uniformly quantified color space. Also, in Lab the color difference is quantified as delta E, the distance in two point in 3D Lab color space [59]. The distance between 3D Lab color space is depicted as square root sum of squared of each Lab color axis. If delta E is same for different color set, then they have equivalent color difference in human perception.

When the colored prostheses are exposed to UV and moisture, degradation in color and mechanical property are induced by direction attack of UV on molecular structure and free radical [60]. If weathering result in mechanical failure or highly noticeable disharmony in color with patient skin color at boundaries, the degraded prostheses required to be replaced [61]. Thus, to guarantee the life span of prostheses, the 3D printed prostheses was tested on UV and moisture induced weathering condition in color and mechanical properties.

4.3. Material and Methods

4.3.1. Particle size and Stability Control for Lake Pigment Binders

To use with printhead for droplet generation, particle size and stability conditions are required to be satisfied for dispersion. To make lake pigments to dispersion for CMY color 3D printing, surface treatment with wet ball milling was conducted. Blue lake #1, red lake pigment #28, and yellow lake pigment #5 (MakingCosmetics Inc) were used to consist CYM color system. To prepare each of pigment dispersion binder, the surface treatment in following steps was conducted. First, a pigment was dispensed to polystyrene dish and air plasma treated for 1minute

with Harrick air plasma cleaner (Harrick Plasma, Ithaca, New York). Then, the plasma treated pigment with polystyrene was inserted to borosilicate container. Octyl silane treatment solution with 98 wt% HPLC grade ethanol (Sigma-Aldrich), 1 wt% DI water, and Triethoxy(octyl)silane (Sigma-Aldrich) 1 wt% was mixed to glass vial and held for one hour for hydrolysis. For the comparison of effect of octyl silane treatment, (3-Mercaptopropyl)trimethoxysilane (Sigma-Aldrich), Trimethoxy Propyl Silane (Sigma-Aldrich), Trimethoxy Vinyl Silane (Sigma-Aldrich), and Titanium Isopropoxide (Sigma-Aldrich) were surface treated with same procedure and wet ball milled. The octyl silane treatment solution was poured to the nitrogen purged container in same mass amount of lake pigment. The container was purged with nitrogen and placed on oven with 40 degree Celsius for 24 hours. The octyl silane solution was vaporized and treated surface of pigments to lipophilic. Then octyl silane modified pigment was dispensed to conical tube and prepared for wet ball milling. For wet ball milling, 45 wt% HPLC grade ethanol, 45 wt% DI water, 5 wt% PVP, and 5 wt% octyl silane treated pigments was mixed to 30g of solution and vortexed. Then the pigment solution was dispensed to alumina container with 1mm and 2mm zirconia ball for wet-ball milling. The solution was mounted to benchtop planetary ball mill (MTI Corporation. Inc, Richmond, CA) and operated in 40Hz, 1000min condition. The wet ball milled pigment dispersion was collected and diluted for binder. The particle size of ball milled pigment was characterized with Coulter N4 analyzer of submicron particle sizes (Coultronics, Hialeah, Florida), to check if the particle size satisfy submicron size required for inkjet printhead system [62].

The binder composition for cyan pigment binder was 15 wt% pigment dispersion, 15 wt% acetone, 15 wt% isopropanol (Sigma Aldrich) and 30 wt% ethanol, 18 wt% DI water, 5% buffer solution, 0.5 wt% PVP, 1.5 wt% Pluronic® F-68. The binder composition for yellow and magenta pigment binder was 30 wt% pigment dispersion, 15 wt% acetone, 15 wt% isopropanol (Sigma

Aldrich) and 30 wt% ethanol, 3.0 wt% DI water, 5% buffer solution, 0.5 wt% PVP, 1.5 wt% Pluronic® F-68. For buffer solution, 0.2M sodium phosphate mono basic in DI water, 0.2 M sodium phosphate monobasic with 0.4 M sodium phosphate dibasic in DI water, and 1.4 M acetic acid was added to each of sample group to adjust pH of solution and its effect on stability. The binder solution for printing was prepared with sodium phosphate monobasic and dibasic and sequentially filtered with 1-microns polytetrafluoroethylene and 0.2-microns polyvinylidene fluoride membrane filter. For control binder condition group, buffer solution and additional Pluronic F-68 were substituted to equivalent weight percentage of DI water and filtered only with 0.45 microns polytetrafluoroethylene filter. The stability was characterized as zeta potential with Malvern Zetasizer Nano (Malvern Instruments, Worcestershire, UK). For the stable operation of dispersion at printhead, particle required to be charged with high enough negative zeta potential to prevent fouling on to negatively charged membrane such as polyimide of printhead [63, 64]. For control binder condition group, buffer solution and additional Pluronic F-68 were substituted to equivalent weight percentage of DI water and filtered only with 0.45 um polytetrafluoroethylene filter.

4.3.2. Full Color 3D printing for Color Space Mapping and Skin Color Printing

For full color 3D printing, prepared CYM color binder and clear binder was used. The binder composition for clear binder was 15 wt% acetone, 15 wt% isopropanol (Sigma Aldrich) and 38.5 wt% ethanol, 26.5 wt% DI water, 5% buffer solution 1 wt% PVP. Then clear binder solution was filtered with 0.2um Polytetrafluoroethylene filter. To print full color parts with binder jetting approach, Z510 printer was utilized. Polymer coating ratio 12.5% with extra 20% amount of PVB B-98 powder was used for the printing. First, build and feed platform of Z510 printer were lowered to avoid interference. Then prepared printheads were installed on the fast axis assembly.

The powder was set on the feed piston. Then the powder was packed using flat acrylic plate. The powder was spread by the roller in fast axis and repeating built in spreading function. 0.1mm layer thickness and 21.7% uniform binder saturation with monochromatic binder option was used for 3D printing. To build designed parts, the printer spread a single layer of powder and deposited solvent based binder to dissolve coating on the powder which leaded to connection between powder. This process was repeated until the last layer of porous printed part was printed. The printed parts were dried in the 3D printer for 24 hours to prevent crack or warping. The powder encapsulating parts was carefully removed in the post processing unit of Z510 printer with air gun in 5kPa pressure and brush. The color printed parts were infiltrated with pressure-vacuum sequential infiltration process with 25% silicone infiltrant condition.

To map basic color space, hex shaped color parts with cyan, magenta, yellow, blue, red, green, white, and black were printed. Averaged basic skin color set from the five ethnic group reported in previous silicone skin color samples[39] were printed to check availability of skin color 3D printing. The color of printed color was measured with CM-2600D spectrophotometer (Konica Minolta Sensing Americas, New Jersey) in D60, 2-degree observer, Lab color space condition. For full color 3D printing, 3D ear model dissected from Human Head 3D model (Grabcad Library, Cambridge, Massachusetts) was used as base model and colored in Zbrush (Pixologic) 3D model editing program.

4.3.3. UV-Moisture Induced Accelerated Weathering for Degradation of Color

Color degradation of maxillofacial prostheses is one of the major failure mechanism [61] and resulted by degradation in matrix and degradation in pigment. About accelerated color degradation in 60 ℃ and moisture, 1.4 times of acceleration regarding natural weathering condition for same energy of UV radiation was observed [65]. The color samples were exposed to

24 hours in 60 ℃ and 28 W/(m^2 • nm) of radiation with Black-Ray UV bench lamp (UVP, Upland, California), so that equivalent energy in QUV testing of 880 hours condition [66]. Considering accelerated weathering factor, this weathering condition was equivalent to 4hours/day exposure for 1.6 years in Florida [67]. Conventional prostheses possess 1-2 years of replacement cycle [68] and this weathering condition simulate the color change of the maxillofacial prostheses on its life span. Change in color by degradation was characterized the color difference, delta E. The color before weathering was measured and compared with color after weathering condition based on calculated delta E for each of the color [69].

4.3.4. UV-Moisture Induced Accelerated Weathering for Degradation of Mechanical Property

The fabricated prostheses should have weathering and fatigue resistance to survive in daily routine use. Iso 37 type 4 tensile samples were same UV and moisture exposure condition for color degradation. The weathering acceleration factor for mechanical property was 1 [70] and it was equivalent to 4hours/day exposure for 1.15 years in Florida [67]. Degradation of silicone composite involved degradation of silicone matrix [71] and invasion of moisture between interface [72]. For the printed parts containing PVB, separation between PVB and silica is also possible due to invasion of moisture . The weathering exposed samples were tested with 0.5 Mpa and 1 Mpa of 1 million cycles of tensile fatigue loading in 10 Hz by Instron E1000 (Instron, Norwood, Massachusetts) because the major stress at wearing of silicone prostheses was simulated at 0.5 Mpa loading with 100% of elongation. The weathering exposed samples were also checked in tensile testing with 5mm/s of displacement rate by Instron5564 (Instron) to observe change in elongation at break and tensile strength depending on weathering condition. The UV and moisture weathered samples after 1 million cycle of 1 Mpa fatigue loading and tensile loading were

observed with Nova 230 SEM in Low Vacuum Detector, 50 Pa Vacuum pressure, and water vapor condition.

4.4. Result and Discussion

4.4.1. Characterization of Cyan, Magenta, Yellow Dispersion for Full-Color 3D printing

In characterization of pigment binder solution, the particle size change of wet ball milled particle depending on surface treatment were observed on Fig.4-1. Original control group without any treatment and ball milled condition without surface treatment showed particle exceed 2000 nm size. Among the surface treatment condition groups, octyl silane treatment show lowest ball milled particle size on yellow lake pigment binder with 247 nm median particle size on yellow lake pigment. Thus, octyl silane treatment successfully hindered the re-agglomeration by increasing lipophilicity and hydrophobicity. By applying octyl silane to cyan and magenta pigment, particle size condition below 1000 nm condition was achieved.

On the octyl silane treated pigment binder concentration, zeta potential was controlled to increase stability. The control groups of magenta and yellow binder solution were positively charged as noted on Fig.4-2. Proper pH range required for octyl silane treatment pigment particle was basic condition over pH 7, and combination of buffer and additional surfactant with filtering changed the zeta potential of binder solution to negatively charged direction. The highest negatively charged condition was changed -25 mv on magenta pigment dispersion. Thus, the control of stability of pigment binder solution was available and CMY pigment dispersion binders were ready for printing.

4.4.2. Characterization of Color for Silicone 3D printed parts

To check distortion in color space and available basic colors, color sample sets were printed and measure with spectrophotometer as shown on Fig. 4-3 and Fig. 4-4. Among basic CMY colors,

magenta shows largest distortion as noted twice larger delta E compared to that of cyan color as indicated in Table 4.1. White to black color difference in brightness, L indicates the range of possible brightness of printed samples as 54.5-76.9. White color showed least distortion in color among basic color printed samples.

On skin color set, major direction in color bias was observed. The printed skin sample set showed brighter (+L) , less red (-a), and less yellow (-a) than intended color, which suggest the direction of possible color compensation for printing as shown on Table 4.2. Thus, to print the brightly colored 3D full color ear prosthesis, the prosthesis was painted darker color than intended color. Lab (40, 8.4, 12.8) for basic color for base skin color, (42.8, 9.2, 16.7) for yellow highlighted ear antihelix, (26.2, 20.3, 11.8) for red highlighted ear helix region. All color used to paint in the 3D model editor was extremely darker than intended color as indicated on Fig. 4-4. The colors were converted in D60 2-degree observer condition for RGB and used for painting ear. The full color 3D ear prosthesis was printed with intended distribution, gradation and smooth transition of color which required for prostheses to match with skin shade around facial defect. Thus, binder jetting approach based on polymer coated silica treated silicone powder and lake pigment dispersion allowed full color 3D printing with silicone which other 3D printing technology has limitation on it.

4.4.3. Color Degradation of Full Color 3D printed parts in Accelerated Weathering

On previous step, we confirmed possibility of full color 3D printing on new silicone powder based binder jetting approach. In accelerated weathering testing, the change in color of 3D printed sample on accelerated weathering condition was tested. The weathering time is equivalent to 1.6 years use in Florida and the color degradation in yellow in UV and moisture condition was less than one sixth of reported value in equivalent weathering condition [66]. Because the yellow

pigment is one of the important base pigment to create skin shades, weathering resistance of yellow pigment significantly effects on stability of skin colors. Skin color set showed acceptable range of color degradation in UV and moisture condition and UV only condition on Fig. 4-5 and Fig. 4-6. Delta E value for both of condition below 12, which is the reported value for conventional material system and half of starch-silicone printed skin color samples by outdoor weathering in 6 weeks in Manchester [22]. One of the possible assumption regarding this case is silica in 3D printed parts act as a opacifier to protect pigment from UV [66]. UV only condition showed less color change compared to UV and moisture condition. Moisture were possible to change to radicals to attack pigment and silicone [60]. Thus, even though the 3D printed prostheses have enough resistance to UV to survive for 1.6 years, but additional care or protection from UV will extend the life span of them.

4.4.4. Mechanical Property Degradation of Silicone printed parts in Accelerated Weathering

To test the mechanical property degradation by UV and moisture condition and UV only accelerated weathering condition, tensile test and fatigue test were conducted. Tensile testing result indicate no significant degradation in elongation at break and tensile strength on Fig. 4-7, which governs toughness of material and fracture by crack generation [73].

In fatigue testing, all weathered sample in 1MPa cyclic tensile loading condition did not failed in one million of fatigue loading cycle on Table 4-3. However, the control group without weathering failed at about 110,000 cycles. In previous study about weathering of silicone suggested additional cross-linking induced by UV [66] and silicone matrix in 3D printed parts was possible to show UV induced cross linking behavior. All samples in 0.5 MPa cycling tensile loading condition did not failed at one million cycle of loadings, which was quite exceeding requirement, 730 cycle for failure with 1-2times of tensile loading due to wear on and off behavior

of maxillofacial prostheses per day. In SEM images on Fig. 4-8, did not show significant development or delamination of material on sample after UV and moisture induced weathering and one million cycle of 1MPa fatigue loading. Thus, UV and moisture weathering will not lead to failure of silicone powder based maxillofacial prostheses for at least 1.16 years.

4.5. Conclusion

In this study, full color 3D printing was achieved based on lake pigment dispersion in organic solvent, and weathering resistance of silicone powder 3D printed parts was confirmed. Octyl silane to increase lipophilicity, wet ball milling, buffer solution with pH adjustment, and additional filtering strategies contributed to fabrication of stable CMY color binder system. Skin color samples and proof of concept full color silicone prostheses were successfully printed with organic solvent CMY color binder system and binder jetting approach. In weathering test, color degradation of 3D printed samples was on acceptable range on 1.6 years equivalent weathering condition. Mechanical property after weathering showed no significant degradation in property after 1.15-year equivalent weathering test condition. Therefore, 3D printing of full color weathering resistant silicone maxillofacial prostheses was achieved based on polymer coated silicone powder and organic solvent based lake pigment dispersion system.

4.6. Figures

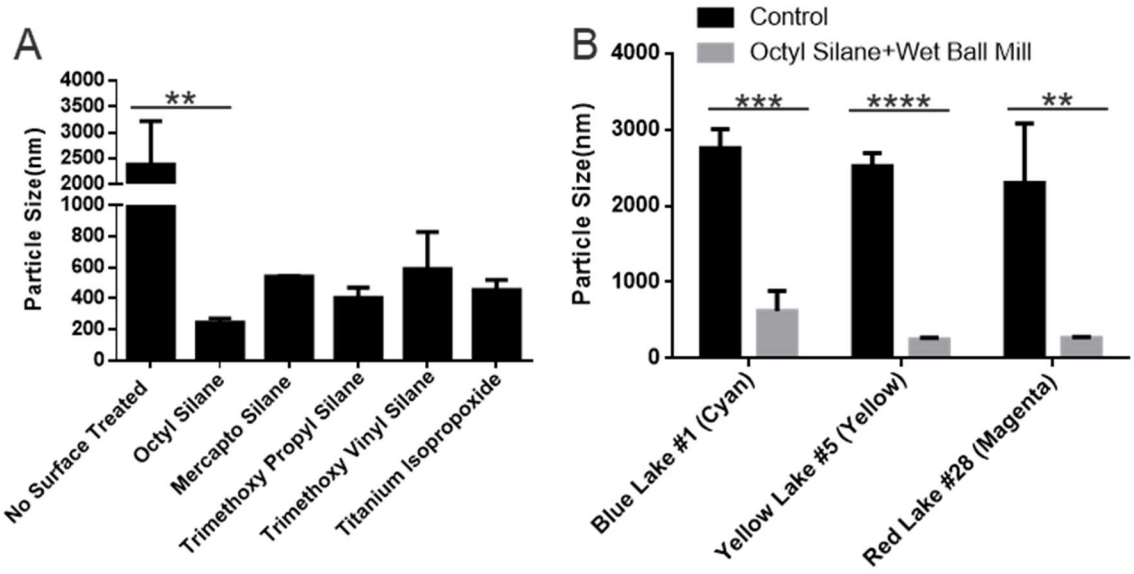

Figure 4-1. Dynamic Laser Scattering Particle Size analyzed dispersion for Full Color binder. (A) Comparison of Effect of surface treatment for Yellow Lake Pigment on Particle Size. (B) Effectiveness of Octyl Silane and Wet Ball Milling on CMY Color Binder dispersion.

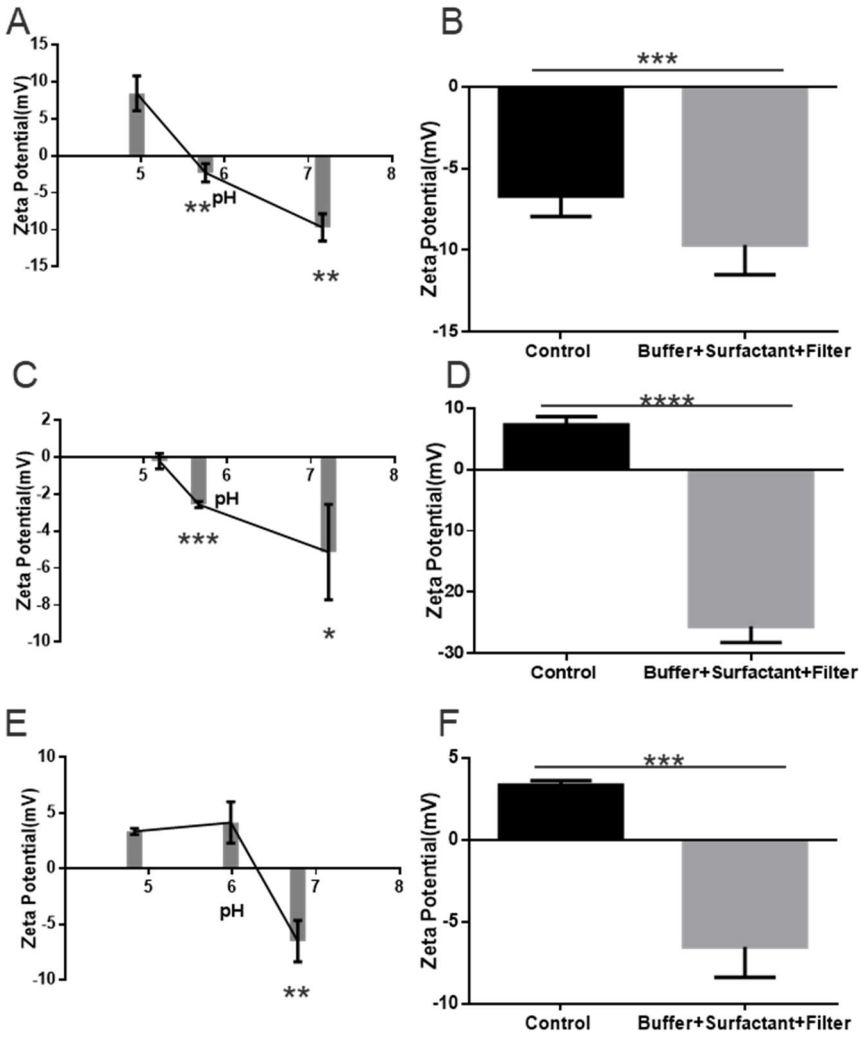

Figure 4-2. Zeta Sizer Dispersion Stability Measurement for Depending on pH and treatment (A-B) Cyan. (C-D) Magenta. (E-F) Yellow.

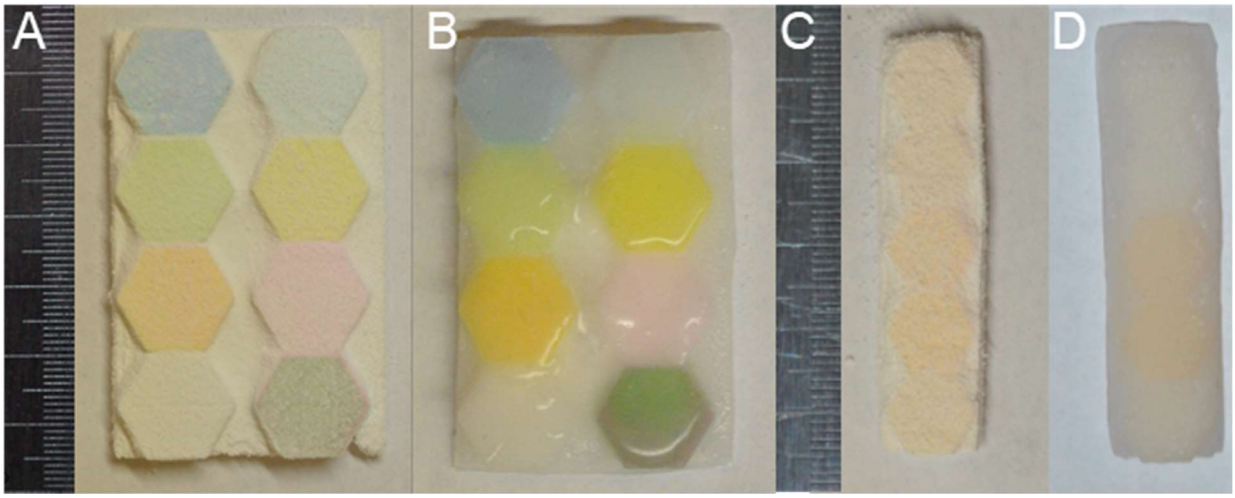

Figure 4-3. Printed Basic Color Space and Skin Color Samples. (A) Basic Color Samples Before Silicone Infiltration. (B) Basic Color Samples After Silicone Infiltration. (C) Skin Color Samples Before Silicone Infiltration. (D) Skin Color Samples After Silicone Infiltration.

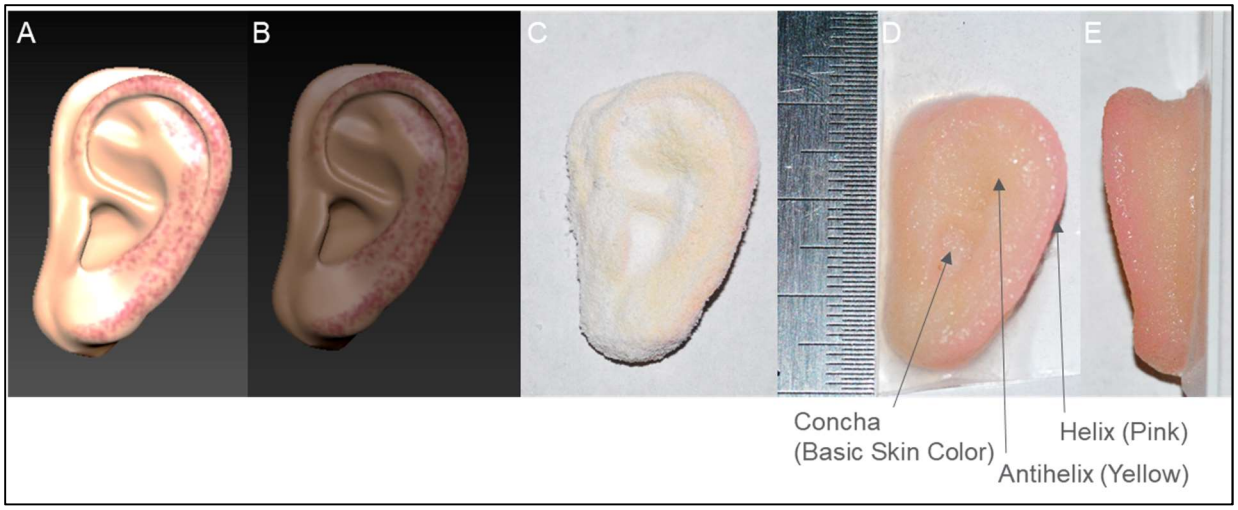

Figure 4-4. Fabrication of Direct 3D Printed Full Color Ear Prosthesis. (A) Intended Full Color Ear Prosthesis. (B) Color Compensated Ear Prosthesis. (C) Printed Ear Prosthesis before Silicone Infiltration. (D) Printed and Infiltrated Full Color Ear Prosthesis. (E) Side View of Full Color Ear Prosthesis

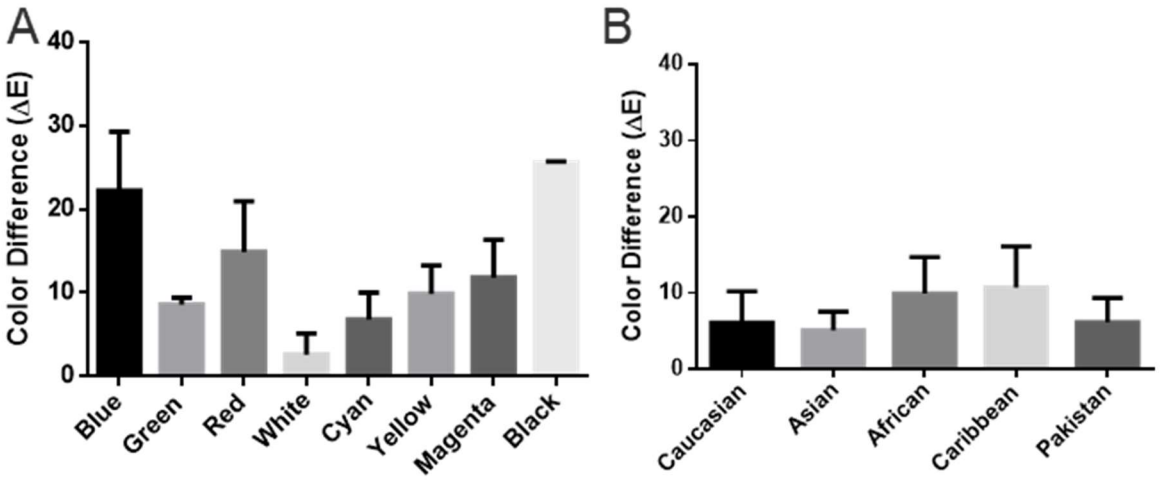

Figure 4-5. UV and Moisture Combined Accelerated Weathering on Color Samples. (A) Basic Color Set. (B) Skin Color Set.

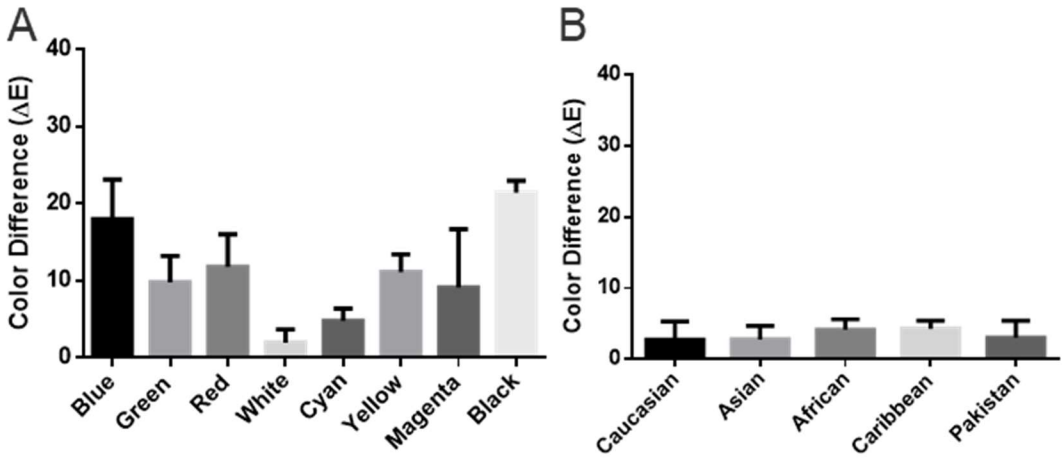

Figure 4-6. UV only Induced Accelerated Weathering on Color Samples. (A) Basic Color Set. (B) Skin Color Set.

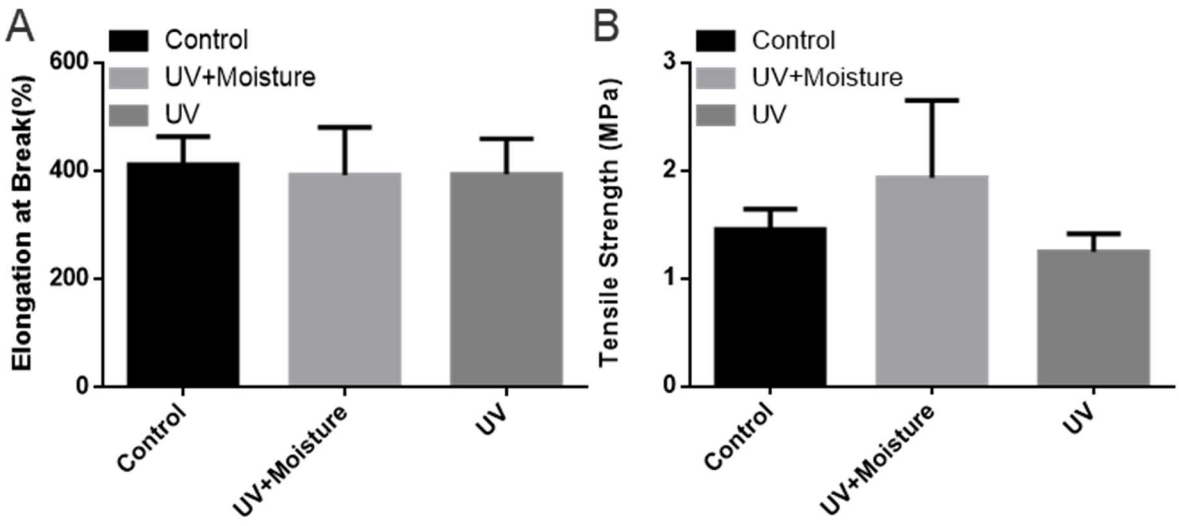

Figure 4-7. UV and Moisture Combined Accelerated Weathering on Tensile Properties (A)Elongation at Break. (B) Tensile Strength.

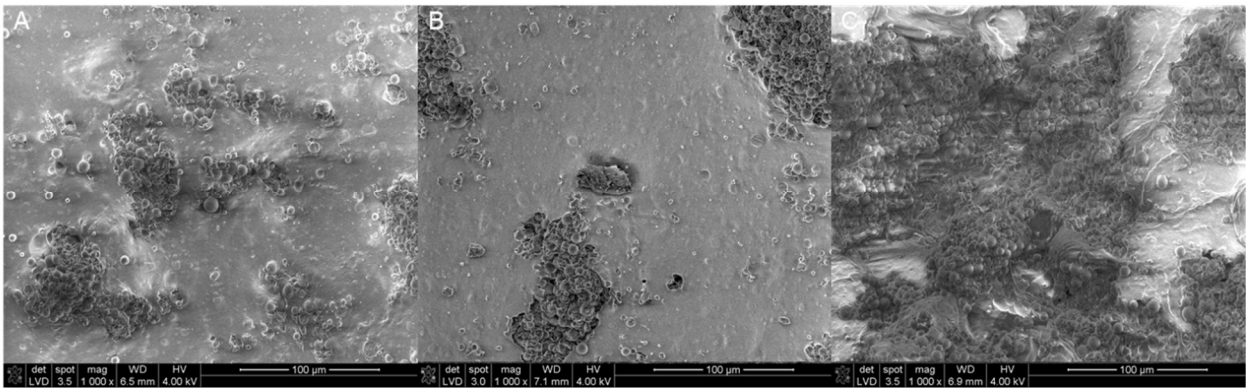

Figure 4-8. Scanning Electron Microscopy on UV and Moisture Weathered and Fatigue Loaded sample (A) Original Sample without Weathering. (B) Weathered and tested with 1Mpa, 1 million cycle of fatigue loading. (C) Fractured Sample by Tensile Stress.

4.7. Tables

Table 4-1. Lab Color Space for Basic Color Set.

	L	a	b	ΔL	Δ a	Δ b	Δ E
Blue	64.47	-10.00	-15.83	32.2	-89.2	92.0	132
Green	75.20	-12.23	20.52	-12.5	74.0	-62.7	98
Red	73.81	-0.66	35.06	20.6	-80.8	-32.2	89
White	76.85	-1.31	-1.62	-23.2	-1.3	-1.6	23
Cyan	69.25	-4.35	-4.69	-21.9	43.7	9.4	50
Yellow	75.75	-9.06	37.11	-21.4	12.5	-57.4	62
Magenta	75.54	8.88	-4.66	15.2	-89.4	56.2	107
Black	54.46	-13.23	15.46	54.5	-13.2	15.5	58

Table 4-2. Lab Color for Skin shade Set and Difference with Reported Value.

	L	**a**	**b**	**ΔL**	**Δ a**	**Δ b**	**Δ E**
Caucasian	69.52	-1.41	7.19	4.69	-9.41	-9.54	14
Asian	69.75	-0.77	15.14	8.30	-6.27	-2.46	11
African	69.74	0.21	17.14	29.41	-8.43	4.61	31
Caribbean	70.15	-0.20	10.55	26.90	-8.70	-8.05	29
Pakistan	71.60	-0.55	7.14	11.85	-8.75	-9.86	18

Table 4-3. Tensile Fatigue Cyclic Loading Test on Samples exposed to Accelerated Weathering.

	Control	**UV+ Moisture**	**UV**
1 Mpa	1.1 ±1.1 (10^5cycles)	>10^6 cycles	>10^6 cycles
0.50 Mpa (100%Elongation)	>10^6 cycles	>10^6 cycles	>10^6 cycles

Chapter 5. Conclusion and Future Directions

5.1. Conclusions

The objective of this project was to develop a technology to direct 3D printing silicone with full color availability, high flexibility, and weathering resistance in order to improve quality of life for patients with head and neck defects. To achieve this goal, customized polymer coated silica treated silicone powder by spray drying, compatible organic solvent based CMY color binder, and sequential biphasic infiltration process were developed. In binder jetting process, full color porous parts are printed with polymer coated silicone powder and CMY color binder, and infused silicone resin to fill the pore in pressure and vacuum infiltration process to turn them to fully dense parts. Chapter 2 describes testing of proper polymer coating material for silicone powder and compatible binder system. Chapter 3 demonstrates control of spray dried particles based on Ohnesorge number and proves direct silicone 3D printing of maxillofacial prostheses in one color. Chapter 4 shows surface modified, particle size controlled, stabilized lake pigment in organic solvent binder system for full color 3D printing and weathering resistance of printed parts. Full color 3D printing of skin color and ear prosthesis was achieved by customized CMY color binder for silicone powder. Weathering resistance in color and mechanical property was confirmed at accelerated weathering condition and mechanical property testing.

Current limitation of this technology is narrow color range and color calibration. The color range of CMY color binder is not enough to print dark skin color such as that of African American and Caribbean. In addition, color distortion on basic colors for color space, and skin colors was observed. To print color corrected samples, statistical approach to evaluate and calibrated color is required.

5.2. Future Directions

The full color 3D printing material system was developed for direct 3D printing of silicone maxillofacial prostheses, but only a monotonous printed prosthesis was tested. Clinical testing of full color 3D printed prostheses gives opportunities to collect more detailed feedback about them from patient, clinical doctors, and technicians. Testing of skin color matching strategy for digitally constructed model helps to engineer detailed procedure for digital based process of maxillofacial prostheses. Statistical model based on Lab color space with polynomial regression [23] may minimize color difference between intended and printed full color prostheses.

To widen color space and stability, additional studies about pigment binder are required. Distortion on each of cyan, magenta, and yellow pigment could be corrected by combined or mixed with other pigments. Additional testing on surfactant, pH [74], and buffer solution for surface charge may help to increase color intensity of printed parts with wider color range. Also, use of UV absorber such as metal nano oxide or benzotriazole based chemical may minimize color degradation in printed parts [75].

In addition, the full color 3D printed silicone parts can be utilized for other applications. Currently, use of rapid prototyping in medical area is growing significantly [76, 77] and direct 3D printing of silicone in full color allows fabrication of suturable and dissectible model for surgery planning and education.

Wearable device or flexible circuit device is one of the recent important research area [78, 79]. Direct 3D printing of silicone with voxel level control allow multi material printing with complex structure, and fully flexible wearable device could be directly printed with additional printhead with conductive or functionality material such as carbon nanotube [80].

References

1. Mitra, A., et al., *Maxillofacial prosthetic materials-an inclination towards silicones.* Journal of clinical and diagnostic research: JCDR, 2014. **8**(12): p. ZE08.
2. Goiato, M.C., et al., *Patient satisfaction with maxillofacial prosthesis. Literature review.* Journal of Plastic, Reconstructive & Aesthetic Surgery, 2009. **62**(2): p. 175-180.
3. Leonardi, A., et al., *Maxillofacial prosthetic rehabilitation using extraoral implants.* Journal of Craniofacial Surgery, 2008. **19**(2): p. 398-405.
4. Anusavice, K.J., C. Shen, and H.R. Rawls, *Phillips' science of dental materials*. 2012: Elsevier Health Sciences.
5. Khindria, S., S. Bansal, and M. Kansal, *Maxillofacial prosthetic materials.* The Journal of Indian Prosthodontic Society, 2009. **9**(1): p. 2.
6. Bibb, R., D. Eggbeer, and P. Evans, *Rapid prototyping technologies in soft tissue facial prosthetics: current state of the art.* Rapid Prototyping Journal, 2010. **16**(2): p. 130-137.
7. He, Y., G.-h. Xue, and J.-z. Fu, *Fabrication of low cost soft tissue prostheses with the desktop 3D printer.* Scientific reports, 2014. **4**: p. 6973.
8. Tse, D., *3-D Printed Facial Prosthesis Offers New Hope for Eye Cancer Patients Following Surgery*, in *American Academy of Ophthalmology*. 2014, American Academy of Ophthalmology.
9. Mohammed, M.I., et al., *Augmented patient-specific facial prosthesis production using medical imaging modelling and 3D printing technologies for improved patient outcomes.* Virtual and Physical Prototyping, 2018. **13**(3): p. 164-176.
10. Liravi, F. and E. Toyserkani, *A hybrid additive manufacturing method for the fabrication of silicone bio-structures: 3D printing optimization and surface characterization.* Materials & Design, 2018. **138**: p. 46-61.
11. Kim, D.S.D. and B.L. Tai, *Hydrostatic support-free fabrication of three-dimensional soft structures.* Journal of Manufacturing Processes, 2016. **24**: p. 391-396.
12. *Carbon Introduces New SIL 30 Silicone Urethane Material.* 2017, 3D Printing Media Network.
13. Ward, R., et al., *In vivo biostability of polysiloxane polyether polyurethanes: Resistance to biologic oxidation and stress cracking.* Journal of Biomedical Materials Research Part A: An Official Journal of The Society for Biomaterials, The Japanese Society for Biomaterials,

and The Australian Society for Biomaterials and the Korean Society for Biomaterials, 2006. **77**(3): p. 580-589.

14. Griesser, H.J., *Degradation of polyurethanes in biomedical applications—a review.* Polymer Degradation and Stability, 1991. **33**(3): p. 329-354.
15. Truby, R.L. and J.A. Lewis, *Printing soft matter in three dimensions.* Nature, 2016. **540**(7633): p. 371.
16. Liravi, F. and E. Toyserkani, *Additive manufacturing of silicone structures: A review and prospective.* Additive Manufacturing, 2018.
17. Abdollahi, S., et al., *Expert-guided optimization for 3D printing of soft and liquid materials.* PloS one, 2018. **13**(4): p. e0194890.
18. Grunewald, S.J., *Wacker announces new silicone 3d printing technology*, in *3D Printing Materials*. August 11, 2015, 3D Print.com.
19. Unkovskiy, A., et al., *Direct 3D printing of silicone facial prostheses: A preliminary experience in digital workflow.* The Journal of prosthetic dentistry, 2018. **120**(2): p. 303-308.
20. Brunton, A., C.A. Arikan, and P. Urban, *Pushing the limits of 3d color printing: Error diffusion with translucent materials.* ACM Transactions on Graphics (TOG), 2015. **35**(1): p. 4.
21. Torabi, K., E. Farjood, and S. Hamedani, *Rapid prototyping technologies and their applications in prosthodontics, a review of literature.* Journal of Dentistry, 2015. **16**(1): p. 1.
22. Zardawi, F.M., *Characterisation of Implant Supported Soft Tissue Prostheses Produced with 3D Colour Printing Technology*. 2013, University of Sheffield.
23. Xiao, K., et al., *Developing a 3D colour image reproduction system for additive manufacturing of facial prostheses.* The International Journal of Advanced Manufacturing Technology, 2014. **70**(9-12): p. 2043-2049.
24. Xiao, K., et al., *Colour Image Reproduction for 3D Printing Facial Prostheses*, in *New Trends in 3D Printing*. 2016, IntechOpen.
25. Berens, A.M., et al., *Computer-aided design and 3D printing to produce a costal cartilage model for simulation of auricular reconstruction.* Otolaryngology–Head and Neck Surgery, 2016. **155**(2): p. 356-359.

26. Alharbi, N., R. Osman, and D. Wismeijer, *Effects of build direction on the mechanical properties of 3D-printed complete coverage interim dental restorations.* The Journal of prosthetic dentistry, 2016. **115**(6): p. 760-767.
27. Muth, J.T., et al., *Embedded 3D printing of strain sensors within highly stretchable elastomers.* Advanced Materials, 2014. **26**(36): p. 6307-6312.
28. LeBlanc, K.J., et al., *Stability of high speed 3D printing in liquid-like solids.* ACS Biomaterials Science & Engineering, 2016. **2**(10): p. 1796-1799.
29. Freeman, I., F. Padley, and W. Sheppard, *Use of silicones in frying oils.* Journal of the American Oil Chemists Society, 1973. **50**(4): p. 101-103.
30. Ramirez, I., E.A. Cherney, and S. Jarayam, *Comparison of the erosion resistance of silicone rubber and EPDM composites filled with micro silica and ATH.* IEEE Transactions on Dielectrics and Electrical Insulation, 2012. **19**(1): p. 218-224.
31. Estevinho, B.N., et al., *Microencapsulation with chitosan by spray drying for industry applications–A review.* Trends in food science & technology, 2013. **31**(2): p. 138-155.
32. *C.-P.I. Surface tension apparatus instruction manual.* Cole Parmer.
33. Hutchings, I.M. and G.D. Martin, *Inkjet technology for digital fabrication*. 2012: John Wiley & Sons.
34. Inzana, J.A., et al., *3D printing of composite calcium phosphate and collagen scaffolds for bone regeneration.* Biomaterials, 2014. **35**(13): p. 4026-4034.
35. Özkol, E., et al., *Development of high solid content aqueous 3Y-TZP suspensions for direct inkjet printing using a thermal inkjet printer.* Journal of the European Ceramic Society, 2009. **29**(3): p. 403-409.
36. Sachs, E., et al., *Three-dimensional printing: the physics and implications of additive manufacturing.* CIRP annals, 1993. **42**(1): p. 257-260.
37. Lewis, D. and D. Castleberry, *An assessment of recent advances in external maxillofacial materials.* The Journal of prosthetic dentistry, 1980. **43**(4): p. 426-432.
38. Trumble, K., *Spontaneous infiltration of non-cylindrical porosity: close-packed spheres.* Acta Materialia, 1998. **46**(7): p. 2363-2367.
39. Zardawi, F.M., et al., *Mechanical properties of 3D printed facial prostheses compared to handmade silicone polymer prostheses.* European Scientific Journal, ESJ, 2015. **11**(12).

40. Kim, H., et al., *PDMS–silica composite membranes with silane coupling for propylene separation.* Journal of Membrane Science, 2009. **344**(1): p. 211-218.
41. Miller, A. and J. Berg, *The prediction of adhesion between polymer matrices and silane-treated glass surfaces in filled composites.* Journal of adhesion science and technology, 2002. **16**(5): p. 495-507.
42. Tandon, G. and G. Weng, *The effect of aspect ratio of inclusions on the elastic properties of unidirectionally aligned composites.* Polymer composites, 1984. **5**(4): p. 327-333.
43. Gillet, A., et al., *Tangible interfaces for structural molecular biology.* Structure, 2005. **13**(3): p. 483-491.
44. Reitz, R.D., *Atomization and other breakup regimes of a liquid jet.* 1978.
45. Post, S.L. and A.J. Hewitt, *Flat-Fan Spray Atomization Model.* 2018.
46. Miyanaji, H., *Binder jetting additive manufacturing process fundamentals and the resultant influences on part quality.* 2018.
47. Miller, A. and J. Berg, *Effect of silane coupling agent adsorbate structure on adhesion performance with a polymeric matrix.* Composites Part A: Applied Science and Manufacturing, 2003. **34**(4): p. 327-332.
48. Heinzen, C., Andreas Berger, and Ian Marison., *Use of vibration technology for jet break-up for encapsulation of cells and liquids in monodisperse microcapsules.* Fundamentals of cell immobilisation biotechnology, 2004: p. 257-275.
49. Wolfaardt, J.F., H.D. Chandler, and B.A. Smith, *Mechanical properties of a new facial prosthetic material.* Journal of Prosthetic Dentistry, 1985. **53**(2): p. 228-234.
50. Meththananda, I.M., et al., *The relationship between Shore hardness of elastomeric dental materials and Young's modulus.* Dental materials, 2009. **25**(8): p. 956-959.
51. Yap, Y., et al. *Investigation of fiber reinforced composite using multi-material 3d printing*. in *Annual International Solid Freeform Fabrication Symposium, Austin, TX, USA*. 2016.
52. Montgomery, P.C. and S. Kiat-Amnuay, *Survey of currently used materials for fabrication of extraoral maxillofacial prostheses in North America, Europe, Asia, and Australia.* Journal of Prosthodontics: Implant, Esthetic and Reconstructive Dentistry, 2010. **19**(6): p. 482-490.
53. Carrot, C., et al., *Polyvinyl Butyral*, in *Handbook of Thermoplastics, red.* 2016, ACRC Press. p. 89-138.

54. *Blue Start SILBIONE ® RTV 4420 A/B*. 2012, SILBIONE.
55. Lei, Y.Y., et al. *Study on Preparation and Factors of Amino Silicone with Low Viscosity*. in *Advanced Materials Research*. 2011. Trans Tech Publ.
56. Bulloch, R.H., et al., *Mapping the broad CMY subtractive primary color gamut using a dual-active electrochromic device.* ACS applied materials & interfaces, 2014. **6**(9): p. 6623-6630.
57. Girdthep, S., et al., *Physico-chemical characterization of natural lake pigments obtained from Caesalpinia Sappan Linn. and their composite films for poly (lactic acid)-based packaging materials.* Dyes and Pigments, 2018. **157**: p. 27-39.
58. Gnanasekharan, V., R. Shewfelt, and M. Chinnan, *Detection of color changes in green vegetables.* Journal of Food Science, 1992. **57**(1): p. 149-154.
59. Davis, B.A., K.H. Friedl, and J.M. Powers, *Color stability of hybrid ionomers after accelerated aging.* Journal of Prosthodontics, 1995. **4**(2): p. 111-115.
60. Eleni, P.N., et al., *Effects of outdoor weathering on facial prosthetic elastomers.* Odontology, 2011. **99**(1): p. 68-76.
61. Ariani, N., *Microbial biofilms on silicone facial prostheses*. 2015: Rijksuniversiteit Groningen.
62. Nir, M.M., et al., *Electrically conductive inks for inkjet printing.* The Chemistry of Inkjet Inks, 2010: p. 225-254.
63. Kirby, B.J. and E.F. Hasselbrink Jr, *Zeta potential of microfluidic substrates: 2. Data for polymers.* Electrophoresis, 2004. **25**(2): p. 203-213.
64. Ayyavoo, J., et al., *Protection of polymeric membranes with antifouling surfacing via surface modifications.* Colloids and Surfaces A: Physicochemical and Engineering Aspects, 2016. **506**: p. 190-201.
65. Lemon, J.C., et al., *Color stability of facial prostheses.* The Journal of prosthetic dentistry, 1995. **74**(6): p. 613-618.
66. Stathi, K., P. Tarantili, and G. Polyzois, *The effect of accelerated ageing on performance properties of addition type silicone biomaterials.* Journal of Materials Science: Materials in Medicine, 2010. **21**(5): p. 1403-1411.
67. McGreer, M., *Weathering Testing Guidebook.* Chicago, USA: Atlas Electric Devices Company, 2003.

68. Visser, A., et al., *Fate of implant-retained craniofacial prostheses: life span and aftercare.* International Journal of Oral & Maxillofacial Implants, 2008. **23**(1).
69. Olabisi, O. and K. Adewale, *Handbook of thermoplastics*. 2016: CRC press.
70. Sandberg, L.B., *Comparisons of silicone and urethane sealant durabilities.* Journal of materials in civil engineering, 1991. **3**(4): p. 278-291.
71. Wang, L., et al., *Biomechanical properties of nano-TiO2 addition to a medical silicone elastomer: the effect of artificial ageing.* Journal of dentistry, 2014. **42**(4): p. 475-483.
72. Ratner, B.D., et al., *Biomaterials science: an introduction to materials in medicine*. 2004: Elsevier.
73. Singleton, A., et al., *On the mechanical properties, deformation and fracture of a natural fibre/recycled polymer composite.* Composites Part B: Engineering, 2003. **34**(6): p. 519-526.
74. Wen, Z.-Q., et al., *Surface modification of organic pigment particles for microencapsulated electrophoretic displays.* Dyes and Pigments, 2012. **92**(1): p. 554-562.
75. Tran, N.H., M. Scarbecz, and J.J. Gary, *In vitro evaluation of color change in maxillofacial elastomer through the use of an ultraviolet light absorber and a hindered amine light stabilizer.* The Journal of prosthetic dentistry, 2004. **91**(5): p. 483-490.
76. Rengier, F., et al., *3D printing based on imaging data: review of medical applications.* International journal of computer assisted radiology and surgery, 2010. **5**(4): p. 335-341.
77. Lim, K.H.A., et al., *Use of 3D printed models in medical education: A randomized control trial comparing 3D prints versus cadaveric materials for learning external cardiac anatomy.* Anatomical sciences education, 2016. **9**(3): p. 213-221.
78. Kim, J., et al., *Advanced materials for printed wearable electrochemical devices: A review.* Advanced Electronic Materials, 2017. **3**(1): p. 1600260.
79. Kolodzey, L., et al., *Wearable technology in the operating room: a systematic review.* BMJ Innovations, 2017. **3**(1): p. 55-63.
80. Wang, S., et al., *Inkjet printing of conductive patterns and supercapacitors using a multi-walled carbon nanotube/Ag nanoparticle based ink.* Journal of Materials Chemistry A, 2015. **3**(5): p. 2407-2413.